IEEE Access
Multidisciplinary : Rapid Review : Open Access Journal

Received 5 February 2026, accepted 14 February 2026, date of publication 18 February 2026, date of current version 27 February 2026.

Digital Object Identifier 10.1109/ACCESS.2026.3665907

THEORY

Mesh Stability of Uncertain Platoon Vehicles With Cornering Maneuver Using Relative Posture Error Information

JUNSEOK BOO[1], KANGMIN JO[2], AND DONGKYOUNG CHWA[2]

[1]Electronics and Telecommunications Research Institute, Yuseong-gu, Daejeon 34129, South Korea

[2]Department of Electrical and Computer Engineering, Ajou University, Suwon 16499, South Korea

Corresponding author: Dongkyoung Chwa (dkchwa@ajou.ac.kr)

This work was supported in part by the National Research Foundation of Korea (NRF) grant funded by the Korea Government (MSIT) under Grant RS-2023-NR076548 and in part by the Institute of Civil Military Technology Cooperation funded by 565 the Defense Acquisition Program Administration and Ministry of Trade, Industry and Energy of Korean 566 Government under Grant 23-CM-TC-13.

ABSTRACT This paper presents a robust bidirectional platoon control method based on coupled relative posture errors to achieve mesh stability of connected vehicles under kinematic and dynamic disturbances. Platoon control for connected and automated vehicles must guarantee safe intervehicle distances and desired heading angles on a two-dimensional (2D) plane, even in the presence of modeling uncertainties and external disturbances. However, most existing studies focus on string stability in either the longitudinal or lateral direction; consequently, bidirectional error propagation on a plane, combined kinematic and dynamic disturbances, and path departure during curved maneuvers are not sufficiently addressed. To overcome these limitations, this paper proposes a robust platoon control framework that guarantees mesh stability and asymptotic convergence of relative posture errors to zero using only relative posture information. Coupled relative posture error dynamics are derived to analyze error propagation on a 2D plane, and a novel robust bidirectional platoon controller employing an adaptive integral sliding mode disturbance observer (AISMDOB) is proposed to ensure asymptotic convergence of both relative spacing and heading angle errors to zero while compensating for kinematic and dynamic disturbances. In addition, an extended look-ahead strategy based on relative posture errors is introduced to prevent path departure during curved maneuvers while relying solely on local onboard sensors instead of global positioning information. Simulation and experimental results demonstrate that the proposed method reduces average relative spacing errors by approximately 29% in simulation and 25% in experiments, and heading angle errors by approximately 9% and 29%, respectively, compared with existing methods.

INDEX TERMS Adaptive integral sliding mode disturbance observer (AISMDOB), coupled relative posture error dynamics, extended look-ahead, mesh stability, robust bidirectional platoon control.

NOMENCLATURE

α_{i-1}	Circular arc angle where $i \in \{1, \cdots, n\}$ and n is the number of vehicles.
γ_{pi}	Unknown bounded constant where the subscript p represents x, y, and θ.
δ_{vi}, $\delta_{\omega i}$	Unknown kinematic disturbances.
δ_{ai}	Unknown dynamic disturbances.
Δ_{xi}, Δ_{yi}, $\Delta_{\theta i}$	Lumped kinematic disturbances.
Δ_{vi}	Lumped dynamic disturbances.
ε_{pi}	Estimation error of the AISMDOB.
κ_{i-1}	Curvature of the preceding vehicle path.
Φ_{xi}, Φ_{yi}, $\Phi_{\theta i}$	Known terms in the coupled relative posture error dynamics.
ω_{ri}, ω_{li}	Right and left wheel velocity inputs.
e_{xi}, e_{yi}, $e_{\theta i}$	Relative posture errors.
$\bar{e}_{xi}$, $\bar{e}_{yi}$, $\bar{e}_{\theta i}$	Coupled relative posture errors.
s_{pi}, $\bar{s}_{pi}$	Sliding surfaces of the AISMDOB.
u_i, ω_i	Longitudinal control input and angular velocity control input.
v_i	Longitudinal velocity.

The associate editor coordinating the review of this manuscript and approving it for publication was Zhiguang Feng.

v_{psei}, θ_{psei}	Pseudo longitudinal velocity and pseudo heading angle.
x_i, y_i, θ_i	Posture variables of the i-th vehicle, including positions x_i, y_i, and heading angle θ_i.
$x_{di}, y_{di}, \theta_{di}$	Target posture variables of the i-th vehicle.

I. INTRODUCTION

Platoon control has attracted widespread interest due to its potential to improve road capacity and fuel efficiency [1], [2], [3], [4]. Maintaining a safe intervehicle distance is essential in platoon control, but tight formation control of platoons poses a challenge known as string stability [2]. String stability refers to the stability that prevents disturbances or spacing errors from propagating along a string of vehicles [2], [3], [4]. It has been extensively investigated for longitudinal and lateral platoon control [5], [6], [7], [8], [9], [10], [11], [12], [13], [14], [15].

However, platoon systems operating on a two-dimensional (2D) plane must maintain not only safe intervehicle distances but also desired heading angles when following curved roads and performing maneuvers. Many 2D platoon control methods rely on GPS-based global position information [16], [17], [18], [19], [20], [21], which becomes critical in indoor or complex urban environments where GPS signals are unreliable [22], [23], motivating the use of relative posture information obtained from onboard sensors [23], [24], [25], [26], [27], [28]. In such scenarios, disturbances or spacing errors can propagate in both the longitudinal and lateral directions; therefore, ensuring mesh stability [29] is necessary beyond conventional string stability along a single direction [29], [30], [31], [32], [33].

The key innovation of this paper is the introduction of a novel robust bidirectional platoon control method that simultaneously guarantees asymptotic stability of relative posture error dynamics, including heading errors, and the mesh stability of the platoon system under both kinematic and dynamic disturbances. This study is motivated by three aspects that, to the best of our knowledge, have not been jointly addressed in existing platoon control studies: 1) use of relative posture information instead of global positioning; 2) simultaneous guarantee of asymptotic convergence of relative posture errors and mesh stability under disturbances; and 3) accurate trajectory tracking during cornering maneuvers. In contrast to our previous work [33], which addressed mesh stability based on global position information, the present study derives coupled relative posture error dynamics on a two-dimensional plane using only relative posture information and explicitly addresses both heading angle stability and the path departure problem during curved maneuvers.

Accordingly, the proposed method employs the derived coupled relative posture error dynamics in conjunction with an adaptive integral sliding mode disturbance observer (AISMDOB), as illustrated in Fig. 1. This combination guarantees that the relative posture errors asymptotically converge to zero and ensures the mesh stability of the bidirectional platoon system in the presence of kinematic and dynamic disturbances. Moreover, the coupled error dynamics are formulated based on an extended look-ahead strategy, which prevents the path departure commonly observed in conventional look-ahead platoon control approaches during cornering maneuvers.

The primary objectives of this paper are threefold. First, we derive coupled relative posture error dynamics for platoon vehicles subject to uncertainties on a 2D plane using only relative posture information. Second, we design an AISMDOB-based robust bidirectional platoon control law that guarantees the asymptotic convergence of relative spacing and heading angle errors while compensating for kinematic and dynamic disturbances. Third, we verify the mesh stability and tracking performance of the proposed method through simulations and experiments.

The contributions of the proposed method are as follows:

1) Novel coupled relative posture error variables utilizing relative posture information are introduced, instead of relying on global positions as in [16], [17], [18], [19], [20], [21], and [33]. This formulation enables coupled relative posture error dynamics to ensure both the asymptotic stability of errors and the mesh stability of the bidirectional platoon system.
2) Robust asymptotic convergence of both the spacing errors and heading angle errors to zero is guaranteed, even in the presence of kinematic and dynamic disturbances. This capability overcomes the limitations of previous 2D platoon control studies that either focus solely on spacing error stability [19], [21], [33] or fail to address both types of disturbances simultaneously [23], [24], [25], [28], [29], [30], [31], [32].
3) Accurate tracking is achieved during cornering maneuvers by introducing a target posture based on the curvature of the preceding vehicle path, thereby overcoming the limitations of existing vehicle following methods [23], [26], [32], [34], which tend to deviate from the curved reference path while aiming to maintain a constant straight-line distance behind the preceding vehicle.

The remainder of this paper is organized as follows. Section II reviews related works on platoon control and mesh stability. Section III formulates the coupled relative posture error dynamics. Section IV presents the AISMDOB-based robust bidirectional platoon control method. Section V analyzes simulation and experimental results. Section VI concludes the paper and discusses limitations and future research directions.

II. LITERATURE REVIEW

Longitudinal and lateral control methods have recently attracted much attention in platoon control. Cooperative adaptive cruise control for uncertain bidirectional platoons is proposed in [5], while [6] introduces a leader–follower control strategy to compensate for communication delays under the same topology. Coupled sliding mode control (SMC)

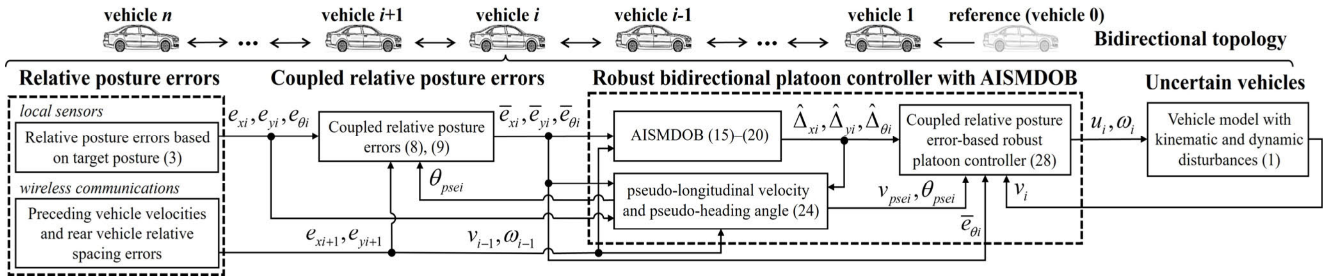

FIGURE 1. Structure of the proposed coupled relative posture error-based robust bidirectional platoon control using AISMDOB.

methods using adaptive laws [7], integral sliding surfaces [8], and finite-time prescribed performance functions [9] have also been developed. In [10], a transmissibility-based monitoring algorithm is proposed for fault detection of longitudinal platoons. A distributed data-driven method is adopted in [11] to address false data injection attacks in platoon vehicles. While these methods effectively ensure longitudinal string stability, lateral string stability in platoon systems has been guaranteed by implementing proportional–derivative [12], H∞ [13], and dynamic gain-scheduling [14] control methods. Additionally, the influence of off-tracking and look-ahead distance on lane-following accuracy has been analyzed along with lateral string stability [15]. However, these studies focus on either longitudinal or lateral control and do not account for error propagation in both directions within a unified stability framework at the same time.

Combined longitudinal and lateral control in 2D platoon systems has been investigated using Bayesian optimization-based optimal control [16], decentralized motion planning for lane changes [17], and event-triggered lane fusion control [18]. In [19], a key point matrix is introduced to enhance trajectory tracking during curved motion. A 2D vehicle dynamic model is decomposed into longitudinal and lateral models in [20] using an arclength parametric transformation to ensure string stability and tracking performance during curved motion. In [21], a novel extended look-ahead method is proposed to avoid cutting-corner behaviors during curved motion. These studies, however, rely on global position information obtained from GPS receivers and do not explicitly consider kinematic and dynamic disturbances affecting vehicle models.

In indoor or complex urban environments, GPS signals are prone to obstruction, hindering the acquisition of global position information [22], [23]. Alternatively, relative posture information obtained from onboard sensors, such as cameras, lidars, and radars, has been investigated in [23], [24], [25], [26], [27], and [28]. In [23], radar and vehicle-to-vehicle communications are used for longitudinal and lateral vehicle following. The relative posture obtained from reference-induced points is used in [24] for an extended look-ahead method with an orientation observer, whereas [25] combines it with a deep deterministic policy gradient algorithm. Robust distance-based predecessor following is implemented in [26] using relative posture obtained from vision sensors. In [27], DoS-attack-resilient platoon control is achieved by fusing lidar measurements with image-based object detection. In [28], a decentralized merging algorithm is proposed for heterogeneous platoon systems equipped with onboard sensors. However, none of these studies consider error propagation in the longitudinal and lateral directions simultaneously.

Error propagation stability in both the longitudinal and lateral directions, called mesh stability, was introduced in [29]. For platoon systems operating on a two-dimensional plane, where disturbances (or spacing errors) can propagate in both directions, mesh stability should be ensured rather than relying solely on string stability, which accounts only for longitudinal or lateral effects. The global exponential and scalable mesh stability of an interconnected look-ahead system is investigated in [30] and [31]. Non-identical longitudinal and identical lateral control methods are combined in [32] to maintain mesh stability. In [33], a robust bidirectional control method for mesh stability is proposed using AISMDOB based on global position measurements. However, [29], [30], [31], and [32] overlook the nonlinearities and uncertainties in vehicle models, such as kinematic and dynamic disturbances that affect real-world vehicle platoons, while [33] still relies on global positioning without considering the stability of heading angles and the path departure problem during cornering maneuvers.

Existing studies have significantly advanced platoon control in terms of longitudinal and lateral string stability, two-dimensional trajectory tracking, and mesh stability. However, most approaches either rely on global position measurements, do not jointly handle kinematic and dynamic disturbances, or fail to simultaneously guarantee mesh stability and asymptotic convergence of relative spacing and heading angle errors using only relative posture information. These gaps motivate the coupled relative posture error-based robust bidirectional platoon control method with AISMDOB proposed in this paper.

III. COUPLED RELATIVE POSTURE ERROR DYNAMICS OF PLATOON VEHICLES WITH KINEMATIC AND DYNAMIC DISTURBANCES

We first detail the platoon vehicle model with kinematic and dynamic disturbances, target vehicle model, and relative

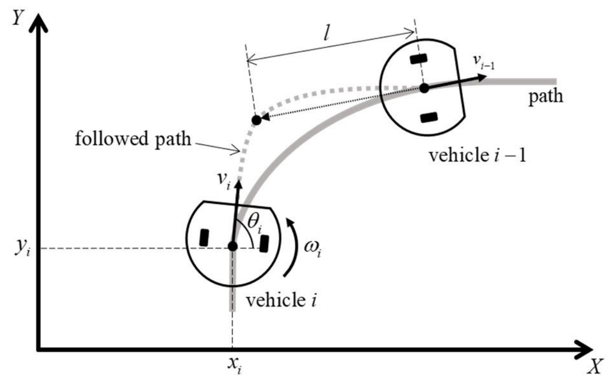

FIGURE 2. Unicycle-type platoon vehicles driving on curved path.

tracking error model between vehicles. Then, the novel coupled relative posture error dynamics are derived.

A. UNCERTAIN PLATOON VEHICLE MODEL AND TARGET POSTURE

A platoon vehicle model can be described using a unicycle-type model [19], [21], [24], [32], as shown in Fig. 2. The platoon vehicle model with kinematic and dynamic disturbances for the i-th vehicle can be expressed as

$$\begin{aligned}
\dot{x}_i &= v_i \cos\theta_i + \delta_{vi} \cos\theta_i \\
\dot{y}_i &= v_i \sin\theta_i + \delta_{vi} \sin\theta_i \\
\dot{v}_i &= u_i + f_i(x_i, y_i, v_i, t) + \delta_{ai} \\
\dot{\theta}_i &= \omega_i + \delta_{\omega i}
\end{aligned} \tag{1}$$

where $i = 1, \cdots, n$; x_i, y_i, and θ_i are posture variables for positions x_i, y_i and heading angle θ_i; v_i is the longitudinal velocity; u_i is the longitudinal control input; ω_i is the angular velocity control input; $f_i(x_i, y_i, v_i, t)$ is an unmodeled nonlinear dynamic function that accounts for rolling resistance frictions, aerodynamic drags, and other aspects; δ_{vi} and $\delta_{\omega i}$ are unknown kinematic disturbances caused by posture uncertainties and slippage; and δ_{ai} represents unknown external dynamic disturbances. The disturbances are estimated and compensated as detailed in Section IV. We introduce Assumptions 1 and 2 for (1) considering real-world vehicle platoon systems.

Assumption 1: The longitudinal and angular velocities and their time derivatives are bounded as $v_i, \omega_i, \dot{v}_i, \dot{\omega}_i \in L_\infty$.

Assumption 2: The unknown disturbances and their time derivatives are bounded as $\delta_{vi}, \delta_{\omega i}, \delta_{ai}, \dot{\delta}_{vi}, \dot{\delta}_{\omega i}, \dot{\delta}_{ai} \in L_\infty$.

Remark 1: Assumption 1 is valid because the states in (1) are physically bounded owing to the saturation of inputs and outputs in the vehicle actuators. In addition, Assumption 2 has been validated in practice in [8], [26], [34], and [35] under various types of disturbances, such as constant, harmonic, and ramp disturbances.

Remark 2: Although (1) is a simplification of a real vehicle dynamics, it extends the unicycle-type model commonly used in various studies on 2D platoon control [19], [21], [24], [32] by accounting for practically existing kinematic and dynamic disturbances, as reported in [26] and [34], which are not jointly considered in [19], [21], [29], [30], [31], and [32].

In this study, constant look-ahead distance l between vehicles is imposed. This is achieved through a constant spacing policy, offering numerous advantages such as enhanced traffic capacity and reduced energy consumption [7]. However, when driving along a curved path, simply keeping distance l behind the preceding vehicle in the backward direction (i.e., $-v_{i-1}$ direction) results in a deviation from the path, as illustrated in Fig. 2.

To address this issue, the posture of the target vehicle, as illustrated in Fig. 3, is defined using the circular arc angle α_{i-1} as follows [24]:

$$\begin{aligned}
x_{di} &= x_{i-1} - l\cos\left(\theta_{i-1} - \alpha_{i-1}/2\right) \\
y_{di} &= y_{i-1} - l\sin\left(\theta_{i-1} - \alpha_{i-1}/2\right) \\
\theta_{di} &= \theta_{i-1} - \alpha_{i-1}
\end{aligned} \tag{2}$$

where $\alpha_{i-1} = 2\tan^{-1}(l\kappa_{i-1}/\sqrt{4 - l^2\kappa_{i-1}^2})$ and $\kappa_{i-1} := \omega_{i-1}/v_{i-1}$ is the curvature of the preceding vehicle path that satisfies $l \leq 2/|\kappa_{i-1}|$. With α_{i-1}, the posture in (2) lies on the same curve as the $(i-1)$-th vehicle, as illustrated in Fig. 3, thereby effectively preventing the path departure (cutting-corner) typically observed in conventional look-ahead schemes during cornering maneuvers.

Considering general driving situations of platoon vehicles without sharp cornering maneuvers, Assumption 3 can be introduced as in [19], [21], and [24].

Assumption 3: The circular arc angle and its first- and second-time derivatives are bounded as $\alpha_{i-1}, \dot{\alpha}_{i-1}, \ddot{\alpha}_{i-1} \in L_\infty$.

B. COUPLED RELATIVE POSTURE ERROR DYNAMICS

This study employs relative posture errors between vehicle i and a target vehicle, as shown in Fig. 3, thereby eliminating the need for global position information. The relative posture errors are defined as follows:

$$\begin{bmatrix} e_{xi} \\ e_{yi} \\ e_{\theta i} \end{bmatrix} = \begin{bmatrix} \cos(\theta_{i-1} - \alpha_{i-1}) & \sin(\theta_{i-1} - \alpha_{i-1}) & 0 \\ -\sin(\theta_{i-1} - \alpha_{i-1}) & \cos(\theta_{i-1} - \alpha_{i-1}) & 0 \\ 0 & 0 & 1 \end{bmatrix} \cdot \begin{bmatrix} x_i - x_{di} \\ y_i - y_{di} \\ \theta_i - \theta_{di} \end{bmatrix}. \tag{3}$$

Relative error variables e_{xi}, e_{yi}, and $e_{\theta i}$ are employed in the proposed platoon controller designed later in (24) and (28). These variables can be obtained directly from camera and lidar sensors as in [24] and [25]. This approach provides a practical implementation and cost-effectiveness by using readily available information from cooperative adaptive cruise control.

Remark 3: In practice, the relative posture errors in (3) are obtained from imperfect onboard sensors, which are affected by noise and jitter. The resulting measurement errors are incorporated into the lumped kinematic disturbances within

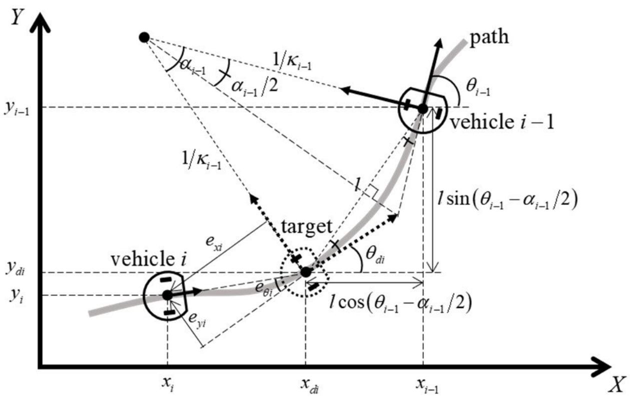

FIGURE 3. **Relative posture errors based on target vehicle.**

the coupled relative posture error dynamics derived later in (10)–(12). These disturbances are assumed to be bounded under Assumptions 1–4 and are estimated and compensated by the proposed AISMDOB-based robust bidirectional platoon controller, as detailed in Section IV.

The relative tracking error model is derived by taking the time derivative of (3) and then applying (2) as follows:

$$\begin{aligned}
\dot{e}_{xi} &= (\omega_{i-1} + \delta_{\omega i-1} - \dot{\alpha}_{i-1})e_{yi} \\
&\quad + \cos(\theta_{i-1} - \alpha_{i-1})\{v_i \cos\theta_i + \delta_{vi}\cos\theta_i - v_{i-1}\cos\theta_{i-1} \\
&\quad -\delta_{vi-1}\cos\theta_{i-1} - l\left(\omega_{i-1} + \delta_{\omega i-1} - \frac{\dot{\alpha}_{i-1}}{2}\right) \\
&\quad \sin\left(\theta_{i-1} - \frac{\alpha_{i-1}}{2}\right)\} \\
&\quad + \sin(\theta_{i-1} - \alpha_{i-1})\{v_i \sin\theta_i + \delta_{vi}\sin\theta_i - v_{i-1}\sin\theta_{i-1} \\
&\qquad -\delta_{vi-1}\sin\theta_{i-1} + l\left(\omega_{i-1} + \delta_{\omega i-1} - \frac{\dot{\alpha}_{i-1}}{2}\right) \\
&\qquad \cos\left(\theta_{i-1} - \frac{\alpha_{i-1}}{2}\right)\} \\
&= v_i \cos e_{\theta i} + \Phi_{xi} + \delta_{xi} \qquad (4) \\
\dot{e}_{yi} &= -(\omega_{i-1} + \delta_{\omega i-1} - \dot{\alpha}_{i-1})e_{xi} \\
&\quad - \sin(\theta_{i-1} - \alpha_{i-1})\{v_i \cos\theta_i + \delta_{vi}\cos\theta_i - v_{i-1}\cos\theta_{i-1} \\
&\quad -\delta_{vi-1}\cos\theta_{i-1} - l\left(\omega_{i-1} + \delta_{\omega i-1} - \frac{\dot{\alpha}_{i-1}}{2}\right) \\
&\qquad \sin\left(\theta_{i-1} - \frac{\alpha_{i-1}}{2}\right)\} \\
&\quad + \cos(\theta_{i-1} - \alpha_{i-1})\{v_i \sin\theta_i + \delta_{vi}\sin\theta_i - v_{i-1}\sin\theta_{i-1} \\
&\quad -\delta_{vi-1}\sin\theta_{i-1} + l\left(\omega_{i-1} + \delta_{\omega i-1} - \frac{\dot{\alpha}_{i-1}}{2}\right) \\
&\qquad \cos\left(\theta_{i-1} - \frac{\alpha_{i-1}}{2}\right)\} \qquad (5) \\
&= v_i \sin e_{\theta i} + \Phi_{yi} + \delta_{yi} \\
\dot{e}_{\theta i} &= \omega_i + \delta_{\omega i} - \omega_{i-1} - \delta_{\omega i-1} + \dot{\alpha}_{i-1} \\
&= \omega_i + \Phi_{\theta i} + \delta_{\theta i} \qquad (6)
\end{aligned}$$

where

$$\begin{aligned}
\Phi_{xi} &= (\omega_{i-1} - \dot{\alpha}_{i-1})e_{yi} - v_{i-1}\cos\alpha_{i-1} - l\left(\omega_{i-1} - \frac{\dot{\alpha}_{i-1}}{2}\right) \\
&\qquad \sin\left(\frac{\alpha_{i-1}}{2}\right) \\
\Phi_{yi} &= (\dot{\alpha}_{i-1} - \omega_{i-1})e_{xi} - v_{i-1}\sin\alpha_{i-1} + l\left(\omega_{i-1} - \frac{\dot{\alpha}_{i-1}}{2}\right) \\
&\qquad \cos\left(\frac{\alpha_{i-1}}{2}\right) \\
\Phi_{\theta i} &= -\omega_{i-1} + \dot{\alpha}_{i-1} \\
\delta_{xi} &= \delta_{\omega i-1}\left\{e_{yi} - l\sin\left(\frac{\alpha_{i-1}}{2}\right)\right\} \\
&\qquad + \delta_{vi}\cos e_{\theta i} - \delta_{vi-1}\cos\alpha_{i-1} \\
\delta_{yi} &= \delta_{\omega i-1}\left\{l\cos\left(\frac{\alpha_{i-1}}{2}\right) - e_{xi}\right\} \\
&\qquad + \delta_{vi}\sin e_{\theta i} - \delta_{vi-1}\sin\alpha_{i-1} \\
\delta_{\theta i} &= \delta_{\omega i} - \delta_{\omega i-1}. \qquad (7)
\end{aligned}$$

Solely stabilizing the relative posture errors for individual vehicles based on (4)–(6) cannot guarantee mesh stability of the platoon system because the platoon vehicles are interconnected and dynamically coupled [10]. To prevent the propagation of relative spacing errors, we propose the following coupled relative spacing errors:

$$\bar{e}_{xi} = \lambda e_{xi} - q e_{xi+1}, \quad \bar{e}_{yi} = \lambda e_{yi} - q e_{yi+1} \qquad (8)$$

where $\lambda > 0$ is a constant, and q is a positive constant such that $\lambda \leq q$ for $i = 1, \cdots, n-1$ and $q = 0$ for $i = n$. These errors use the relative spacing errors of rear vehicle $i+1$ transmitted through vehicle-to-vehicle wireless communications, as illustrated in Fig. 1.

Remark 4: The relationship between the relative spacing errors in (3) and coupled relative spacing errors in (8) can be easily obtained in the form of $\bar{e}_x = Qe_x$ and $\bar{e}_y = Qe_y$ for $e_x := [e_{x1}, \cdots, e_{xn}]^T$, $e_y := [e_{y1}, \cdots, e_{yn}]^T$, $\bar{e}_x := [\bar{e}_{x1}, \cdots, \bar{e}_{xn}]^T$, $\bar{e}_y := [\bar{e}_{y1}, \cdots, \bar{e}_{yn}]^T$, and a nonsingular matrix Q, as provided later in Theorem 1. Therefore, the coupled relative spacing errors in (8) are introduced for easier verification of the mesh stability of the platoon system using the proposed method.

The coupled relative heading angle error can be defined as

$$\bar{e}_{\theta i} = e_{\theta i} - \theta_{psei} \qquad (9)$$

where θ_{psei} is the pseudo heading angle introduced later in (24). If the path followed by vehicles in a platoon is a straight line, θ_{psei} becomes zero, thereby reducing $\dot{\theta}_{psei}$ and $\ddot{\theta}_{psei}$ to zero [26]. Hence, considering not only the boundedness of ω_i and $\dot{\omega}_i$, as specified in Assumption 1, but also that the vehicles follow a smooth path, as described in Assumption 3, we can introduce Assumption 4, as in [26] and [34].

Assumption 4: The pseudo heading angle and its first- and second-time derivatives are bounded as $\theta_{psei}, \dot{\theta}_{psei}, \ddot{\theta}_{psei} \in L_\infty$.

By taking the time derivatives of (8) and (9), the coupled relative posture error dynamics can be derived using (4)–(6) as follows:

$$\begin{aligned}
\dot{\bar{e}}_{xi} &= \lambda v_i \cos e_{\theta i} + \lambda\Phi_{xi} + \Delta_{xi} \qquad (10) \\
\dot{\bar{e}}_{yi} &= \lambda v_i \sin e_{\theta i} + \lambda\Phi_{yi} + \Delta_{yi} \qquad (11) \\
\dot{\bar{e}}_{\theta i} &= \omega_i + \Phi_{\theta i} + \Delta_{\theta i} \qquad (12)
\end{aligned}$$

where $\Delta_{xi} := \lambda\delta_{xi} - q\dot{e}_{xi+1}$, $\Delta_{yi} := \lambda\delta_{yi} - q\dot{e}_{yi+1}$, and $\Delta_{\theta i} := \delta_{\theta i} - \dot{\theta}_{psei}$ represent lumped kinematic disturbances bounded by Assumptions 1–4. The lumped kinematic disturbances are estimated and then compensated using the proposed robust bidirectional platoon controller in Section IV.

Remark 5: Unlike most existing 2D platoon control methods [16], [17], [18], [19], [20], [21], [22], [23], [24], [25], [26], which often focus on controlling either the global or relative posture errors, we formulate the coupled relative posture error dynamics in (10)–(12) and employ them to both stabilize the relative posture errors and achieve mesh stability of the platoon system.

IV. COUPLED RELATIVE POSTURE ERROR-BASED ROBUST BIDIRECTIONAL PLATOON CONTROL USING AISMDOB

In this section, an AISMDOB is developed to estimate the lumped kinematic disturbances. Subsequently, a coupled relative posture error-based robust bidirectional platoon controller is proposed utilizing the developed AISMDOB.

To estimate the lumped kinematic disturbances, we first arrange (10)–(12) as follows:

$$\begin{bmatrix} \dot{\bar{e}}_{xi} \\ \dot{\bar{e}}_{yi} \\ \dot{\bar{e}}_{\theta i} \end{bmatrix} = \begin{bmatrix} \Gamma_{xi} \\ \Gamma_{yi} \\ \Gamma_{\theta i} \end{bmatrix} + \begin{bmatrix} \Delta_{xi} \\ \Delta_{yi} \\ \Delta_{\theta i} \end{bmatrix} \tag{13}$$

where $[\Gamma_{xi}, \Gamma_{yi}, \Gamma_{\theta i}]^T = [\lambda v_i \cos e_{\theta i} + \lambda\Phi_{xi}, \lambda v_i \sin e_{\theta i} + \lambda\Phi_{yi}, \omega_i + \Phi_{\theta i}]^T$. Each row in (13) is expressed for $p = x, y, \theta$ as

$$\dot{\bar{e}}_{pi} = \Gamma_{pi} + \Delta_{pi}. \tag{14}$$

We consider that Δ_{pi} is bounded by $\left\|\Delta_{pi}\right\|_{\infty} < \gamma_{pi}$ for unknown constant γ_{pi} owing to Assumptions 1–4.

Based on (14), the AISMDOB is expressed as

$$\dot{\hat{\bar{e}}}_{pi} = \Gamma_{pi} + \hat{\Delta}_{pi} \tag{15}$$

where $\hat{\bar{e}}_{pi}$ and $\hat{\Delta}_{pi}$ are the estimates of $\bar{e}_{pi}$ and Δ_{pi}, respectively. The integral sliding surface is designed in terms of estimation error $\varepsilon_{pi} := \bar{e}_{pi} - \hat{\bar{e}}_{pi}$ as

$$s_{pi} = \varepsilon_{pi} - \varepsilon_{pi}(0) + \int_0^t \hat{\gamma}_{pi} \tanh\left\{(a_i + b_i\tau)\varepsilon_{pi}\right\} d\tau \tag{16}$$

$$\dot{\hat{\gamma}}_{pi} = \mu_{pi}\left[s_{pi}\tanh\left\{(a_i + b_i t)s_{pi}\right\} + \left|\bar{s}_{pi}\right|(a_i + b_i t)\sec h^2\left\{(a_i + b_i t)s_{pi}\right\}\right] \tag{17}$$

where $a_i, b_i, \mu_{pi} > 0$ are constants, $\hat{\gamma}_{pi}$ is the estimate of the unknown constant γ_{pi}, and $\bar{s}_{pi}$ is a sliding surface given by

$$\bar{s}_{pi} = \upsilon_{pi} + \tanh\left\{(a_i + b_i t)s_{pi}\right\}. \tag{18}$$

Here, auxiliary input υ_{pi} can be obtained from

$$\begin{aligned} \dot{\upsilon}_{pi} = & -\bar{\eta}_{pi} sgn(\bar{s}_{pi}) - s_{pi} + \sec h^2\left\{(a_i + b_i t)s_{pi}\right\} \\ & \cdot\left\langle(a_i + b_i t)\left[\hat{\Delta}_{pi} - \hat{\gamma}_{pi}\tanh\left\{(a_i + b_i t)\varepsilon_{pi}\right\}\right] - b_i s_{pi}\right\rangle \\ & - \hat{\gamma}_{pi}(a_i + b_i t)\sec h^2\left\{(a_i + b_i t)s_{pi}\right\} sgn(\bar{s}_{pi}) \end{aligned} \tag{19}$$

for constant $\bar{\eta}_{pi} > 0$, and its initial condition is selected as $\upsilon_{pi}(0) = 0$ such that the initial conditions of the sliding surfaces satisfy $s_{pi}(0) = \bar{s}_{pi}(0) = 0$. Thus, the reaching phase of the sliding surfaces is eliminated. In addition, $\bar{s}_{pi}$ is introduced to prevent chattering owing to the signum function in (19) by using the concept of backstepping method [35].

Remark 6: The adaptive law in (17) employs the hyperbolic tangent function because it is an odd, smooth, and bounded approximation of the sign function with a bounded derivative, which is convenient for the Lyapunov-based analysis and helps to mitigate chattering. Other smooth bounded nonlinear functions with similar properties could also be used in place of $\tanh(\cdot)$ within the same control structure.

Finally, estimate $\hat{\Delta}_{pi}$ in (17) is designed as

$$\begin{aligned} \hat{\Delta}_{pi} = & \eta_{pi}s_{pi} - \upsilon_{pi} \\ & + \hat{\gamma}_{pi}\left[\tanh\left\{(a_i + b_i t)\varepsilon_{pi}\right\} + \tanh\left\{(a_i + b_i t)s_{pi}\right\}\right] \end{aligned} \tag{20}$$

where η_{pi} is a positive constant.

The estimation performance of the AISMDOB in (15)–(20) is analyzed in Lemma 1.

Lemma 1: (AISMDOB for Estimating Lumped Kinematic Disturbances): Under Assumptions 1–4, the estimation errors obtained by the AISMDOB in (15)–(20) are asymptotically stable in that i) $\bar{s}_{pi} \in L_\infty$, ii) $s_{pi} \in L_2 \cap L_\infty$, iii) s_{pi}, $\dot{s}_{pi}$, and ε_{pi} asymptotically converge to zero, and iv) $\hat{\Delta}_{pi}$ asymptotically converges to Δ_{pi}.

Proof: The proof is omitted here and can be referred to [33]. Unlike the previous AISMDOB [33], which estimates kinematic disturbances only from spacing errors, the proposed method in (15)–(20) is extended to estimate kinematic disturbances arising from relative heading angle errors as well, which can also be proven in a manner similar to [33]. ■

Remark 7: The AISMDOB in (15)–(20) utilizes an adaptive law in (17) to estimate the unknown γ_{pi} while retaining the advantages of the conventional ISMDOB, such as fast convergence and robust performance. This adaptive feature further enhances its applicability to real-world platoon control. The observer gains should be carefully tuned to balance disturbance rejection speed against noise sensitivity. The effectiveness of the AISMDOB is verified in Section V through comparison with the ISMDOB [35].

Next, we propose a coupled relative posture error-based robust bidirectional platoon controller to ensure both the asymptotic stability of (10)–(12) and mesh stability of the bidirectional platoon system depicted in Fig. 1.

The coupled relative posture error dynamics in (10) and (11) are further modified as follows:

$$\begin{aligned} \dot{\bar{e}}_{xi} &= \lambda v_i \cos e_{\theta i} - X_i - k_{xi}\bar{e}_{xi} - \frac{\bar{k}_{xi}^2\bar{e}_{xi}}{\left|\bar{e}_{xi}\right|\bar{k}_{xi} + \exp(-\varsigma t)} + \tilde{\Delta}_{xi} \\ \dot{\bar{e}}_{yi} &= \lambda v_i \sin e_{\theta i} - Y_i - k_{yi}\bar{e}_{yi} - \frac{\bar{k}_{yi}^2\bar{e}_{yi}}{\left|\bar{e}_{yi}\right|\bar{k}_{yi} + \exp(-\varsigma t)} + \tilde{\Delta}_{yi} \end{aligned} \tag{21}$$

by introducing variables X_i and Y_i given by

$$X_i = -k_{xi}\bar{e}_{xi} - \frac{\bar{k}_{xi}^2\bar{e}_{xi}}{|\bar{e}_{xi}|\,\bar{k}_{xi} + \exp(-\varsigma t)} - \lambda\Phi_{xi} - \hat{\Delta}_{xi}$$
$$Y_i = -k_{yi}\bar{e}_{yi} - \frac{\bar{k}_{yi}^2\bar{e}_{yi}}{|\bar{e}_{yi}|\,\bar{k}_{yi} + \exp(-\varsigma t)} - \lambda\Phi_{yi} - \hat{\Delta}_{yi} \quad (22)$$

for constants $k_{xi}, \bar{k}_{xi}, k_{yi}, \bar{k}_{yi}, \varsigma > 0$. Here, $\tilde{\Delta}_{xi} := \Delta_{xi} - \hat{\Delta}_{xi}$ and $\tilde{\Delta}_{yi} := \Delta_{yi} - \hat{\Delta}_{yi}$ are estimation errors that asymptotically converge to zero according to Lemma 1.

Defining the first and second terms on the right-hand side of each row in (21) as $\xi_{xi} := \lambda v_i \cos e_{\theta i} - X_i$ and $\xi_{yi} := \lambda v_i \sin e_{\theta i} - Y_i$, v_i and $e_{\theta i}$ should be adjusted to make ξ_{xi} and ξ_{yi} converge to zero, which is equivalent to making the right-hand sides of

$$\xi_{xi}\cos e_{\theta i} + \xi_{yi}\sin e_{\theta i} = \lambda v_i - X_i\cos e_{\theta i} - Y_i \sin e_{\theta i}$$
$$-\xi_{xi}\sin e_{\theta i} + \xi_{yi}\cos e_{\theta i} = X_i \sin e_{\theta i} - Y_i\cos e_{\theta i} \quad (23)$$

become zero. To this end, the pseudo longitudinal velocity and pseudo heading angle are expressed as

$$v_{psei} = \frac{1}{\lambda}\left(X_i\cos e_{\theta i} + Y_i \sin e_{\theta_i}\right)$$
$$\theta_{psei} = \operatorname{atan2}(Y_i, X_i) \quad (24)$$

where atan2$(\cdot,\cdot)$ is a four-quadrant inverse tangent function satisfying $X_i \sin\theta_{psei} = Y_i\cos\theta_{psei}$. Using (24) and

$$\begin{aligned}\Theta_i &= X_i\sin e_{\theta i} - Y_i\cos e_{\theta i}\\ &= X_i \sin e_{\theta i} - Y_i\cos\theta_{psei} - (\cos e_{\theta i} - \cos\theta_{psei})Y_i\\ &= (\sin e_{\theta i} - \sin\theta_{psei})X_i - (\cos e_{\theta i} - \cos\theta_{psei})Y_i\\ &= 2\sin\left(\frac{\bar{e}_{\theta i}}{2}\right)\\ &\quad \left\{\cos\left(\frac{e_{\theta i}+\theta_{psei}}{2}\right)X_i + \sin\left(\frac{e_{\theta i}+\theta_{psei}}{2}\right)Y_i\right\},\end{aligned} \quad (25)$$

we can reformulate ξ_{xi} and ξ_{yi} as follows:

$$\begin{aligned}\xi_{xi} &= \lambda(v_i - v_{psei})\cos e_{\theta i} + \lambda v_{psei}\cos e_{\theta i} - X_i\\ &= \lambda\bar{e}_{vi}\cos e_{\theta i} + X_i\cos^2 e_{\theta i} + Y_i\cos e_{\theta i}\sin e_{\theta i} - X_i\\ &= \lambda\bar{e}_{vi}\cos e_{\theta i} + (-X_i\sin e_{\theta i} + Y_i\cos e_{\theta i})\sin e_{\theta i}\\ &= \lambda\bar{e}_{vi}\cos e_{\theta i} - \Theta_i\sin e_{\theta i}\\ \xi_{yi} &= \lambda(v_i - v_{psei})\sin e_{\theta i} + \lambda v_{psei}\sin e_{\theta i} - Y_i\\ &= \lambda\bar{e}_{vi}\sin e_{\theta i} + X_i\sin e_{\theta i}\cos e_{\theta i} + Y_i\sin^2 e_{\theta i} - Y_i\\ &= \lambda\bar{e}_{vi}\sin e_{\theta i} + (X_i\sin e_{\theta i} - Y_i\cos e_{\theta i})\cos e_{\theta i}\\ &= \lambda\bar{e}_{vi}\sin e_{\theta i} + \Theta_i\cos e_{\theta i}\end{aligned} \quad (26)$$

where $\bar{e}_{vi} := v_i - v_{psei}$ denotes the longitudinal velocity error. Owing to the equivalence of $\bar{e}_{\theta i} = 0$ and $\Theta_i = 0$ by (25), if $\bar{e}_{vi}$ and $\bar{e}_{\theta i}$ converge to zero, then ξ_{xi} and ξ_{yi} in (26) also converge to zero. To this end, the longitudinal velocity error dynamics are derived from (1) as follows:

$$\dot{\bar{e}}_{vi} = u_i + \Delta_{vi} \quad (27)$$

Algorithm 1 Coupled Relative Posture-Based Robust Bidirectional Platoon Control Using AISMDOB

Input: Relative posture errors e_x, e_y, e_θ; preceding-vehicle velocities v_{i-1}, ω_{i-1}; control parameters.
Output: Control inputs u_i and ω_i.
1: Construct $\bar{e}_x$, $\bar{e}_y$, and $\bar{e}_\theta$ according to (8) and (9).
2: Compute α_{i-1} and its derivative $\dot{\alpha}_{i-1}$ from κ_{i-1}, and then compute Φ_x, Φ_y, Φ_θ using (7).
3: Update AISMDOB states and compute $\hat{\Delta}_{xi}$, $\hat{\Delta}_{yi}$, $\hat{\Delta}_{\theta i}$ using (15)–(20).
4: Compute X_i and Y_i using (22) and the pseudo-variables v_{psei} and θ_{psei} from (24).
5: Compute $\bar{e}_{vi}$ using (27).
6: Determine u_i and ω_i according to (28).
This procedure is executed for each vehicle i in the platoon at every sampling instant.

where $\Delta_{vi} := f_i(x_i, y_i, v_i, t) + \delta_{ai} - \dot{v}_{psei}$ represents the lumped dynamic disturbances and is bounded according to Assumptions 1–4.

Based on (12) and (27), the control inputs to ensure the convergence of $\bar{e}_{vi}$ and $\bar{e}_{\theta i}$ to zero are designed as

$$u_i = -k_{vi}\bar{e}_{vi} - \frac{\bar{k}_{vi}^2\bar{e}_{vi}}{|\bar{e}_{vi}|\,\bar{k}_{vi} + \exp(-\varsigma t)}$$
$$\omega_i = -k_{\theta i}\sin\bar{e}_{\theta i} - \frac{\bar{k}_{\theta i}^2\sin\bar{e}_{\theta i}}{|\sin\bar{e}_{\theta i}|\,\bar{k}_{\theta i} + \exp(-\varsigma t)} - \Phi_{\theta i} - \hat{\Delta}_{\theta i} \quad (28)$$

where $k_{vi}, \bar{k}_{vi}, k_{\theta i}, \bar{k}_{\theta i} > 0$ are constants. The lumped kinematic disturbances in (10)–(12) are effectively compensated by the AISMDOB-based pseudo variables in (24), defined from (22), along with the second line in (28). In addition, the lumped dynamic disturbances in (27) are directly compensated by the first line in (28). This explicit separation of kinematic and dynamic disturbance compensation enhances robustness against modeling errors and external disturbances.

Consequently, substituting (28) into (27) and (12) yields

$$\dot{\bar{e}}_{vi} = -k_{vi}\bar{e}_{vi} - \frac{\bar{k}_{vi}^2\bar{e}_{vi}}{|\bar{e}_{vi}|\,\bar{k}_{vi} + \exp(-\varsigma t)} + \Delta_{vi}$$
$$\dot{\bar{e}}_{\theta i} = -k_{\theta i}\sin\bar{e}_{\theta i} - \frac{\bar{k}_{\theta i}^2\sin\bar{e}_{\theta i}}{|\sin\bar{e}_{\theta i}|\,\bar{k}_{\theta i} + \exp(-\varsigma t)} + \tilde{\Delta}_{\theta i} \quad (29)$$

where $\tilde{\Delta}_{\theta i} := \Delta_{\theta i} - \hat{\Delta}_{\theta i}$ represents the estimation error of $\Delta_{\theta i}$ and asymptotically converges to zero according to Lemma 1.

The proposed control algorithm is summarized in Algorithm 1, and the overall control architecture of the proposed method is illustrated in Fig. 1. The stability and performance properties of the controller defined in (28) are analyzed in Theorem 1.

Theorem 1: (Stabilization of Coupled Relative Posture and Longitudinal Velocity Errors via Robust Bidirectional Platoon Control Using AISMDOB): If $\bar{k}_{xi}$, $\bar{k}_{yi}$, $\bar{k}_{\theta i}$, and $\bar{k}_{vi}$

in (22) and (28) are selected to satisfy $\bar{k}_{xi} > \left|\tilde{\Delta}_{xi} + \xi_{xi}\right|$, $\bar{k}_{yi} > \left|\tilde{\Delta}_{yi} + \xi_{yi}\right|$, $\bar{k}_{\theta i} > \left|\tilde{\Delta}_{\theta i}\right|$, and $\bar{k}_{vi} > |\Delta_{vi}|$, respectively, then coupled relative posture errors $\bar{e}_{xi}$, $\bar{e}_{yi}$, $\bar{e}_{\theta i}$, and longitudinal velocity error $\bar{e}_{vi}$ asymptotically converge to zero for all the vehicles. In addition, the relative spacing errors asymptotically converge to zero as well.

Proof: To demonstrate the asymptotic convergence of $\bar{e}_{xi}$, $\bar{e}_{yi}$, $\bar{e}_{\theta i}$, and $\bar{e}_{vi}$, a Lyapunov candidate function V_i for vehicle i is chosen to be

$$V_i = \frac{1}{2}\bar{e}_{xi}^2 + \frac{1}{2}\bar{e}_{yi}^2 + (1 - \cos\bar{e}_{\theta i}) + \frac{1}{2}\bar{e}_{vi}^2 \tag{30}$$

and its time derivative is derived using (21) and (29) as

$$\begin{aligned}
\dot{V}_i &= \bar{e}_{xi}\dot{\bar{e}}_{xi} + \bar{e}_{yi}\dot{\bar{e}}_{yi} + \sin\bar{e}_{\theta i}\dot{\bar{e}}_{\theta i} + \bar{e}_{vi}\dot{\bar{e}}_{vi} \\
&= \bar{e}_{xi}\left(-k_{xi}\bar{e}_{xi} - \frac{\bar{k}_{xi}^2\bar{e}_{xi}}{|\bar{e}_{xi}|\,\bar{k}_{xi} + \exp(-\varsigma t)} + \tilde{\Delta}_{xi} + \xi_{xi}\right) \\
&\quad + \bar{e}_{yi}\left(-k_{yi}\bar{e}_{yi} - \frac{\bar{k}_{yi}^2\bar{e}_{yi}}{|\bar{e}_{yi}|\,\bar{k}_{yi} + \exp(-\varsigma t)} + \tilde{\Delta}_{yi} + \xi_{yi}\right) \\
&\quad + \sin\bar{e}_{\theta i}\left(-k_{\theta i}\sin\bar{e}_{\theta i} - \frac{\bar{k}_{\theta i}^2\sin\bar{e}_{\theta i}}{|\sin\bar{e}_{\theta i}|\,\bar{k}_{\theta i} + \exp(-\varsigma t)} + \tilde{\Delta}_{\theta i}\right) \\
&\quad + \bar{e}_{vi}\left(-k_{vi}\bar{e}_{vi} - \frac{\bar{k}_{vi}^2\bar{e}_{vi}}{|\bar{e}_{vi}|\,\bar{k}_{vi} + \exp(-\varsigma t)} + \Delta_{vi}\right) \\
&= -k_{xi}\bar{e}_{xi}^2 - k_{yi}\bar{e}_{yi}^2 - k_{\theta i}\sin^2\bar{e}_{\theta i} - k_{vi}\bar{e}_{vi}^2 + \bar{e}_{xi}\left(\tilde{\Delta}_{xi} + \xi_{xi}\right) \\
&\quad + \bar{e}_{yi}\left(\tilde{\Delta}_{yi} + \xi_{yi}\right) + \sin\bar{e}_{\theta i}\tilde{\Delta}_{\theta i} + \bar{e}_{vi}\Delta_{vi} \\
&\quad - \frac{\bar{k}_{xi}^2\bar{e}_{xi}^2}{|\bar{e}_{xi}|\,\bar{k}_{xi} + \exp(-\varsigma t)} - \frac{\bar{k}_{yi}^2\bar{e}_{yi}^2}{|\bar{e}_{yi}|\,\bar{k}_{yi} + \exp(-\varsigma t)} \\
&\quad - \frac{\bar{k}_{\theta i}^2\sin^2\bar{e}_{\theta i}}{|\sin\bar{e}_{\theta i}|\,\bar{k}_{\theta i} + \exp(-\varsigma t)} - \frac{\bar{k}_{vi}^2\bar{e}_{vi}^2}{|\bar{e}_{vi}|\,\bar{k}_{vi} + \exp(-\varsigma t)}.
\end{aligned} \tag{31}$$

The following inequality [36] holds true for $\bar{p} = x, y, \theta, v$:

$$-\frac{\bar{k}_{\bar{p}i}^2(\,\cdot\,)^2}{|\cdot|\,\bar{k}_{\bar{p}i} + \exp(-\varsigma t)} < -\bar{k}_{\bar{p}i}\,|\cdot| + \exp(-\varsigma t). \tag{32}$$

Hence, (31) can be arranged as follows:

$$\begin{aligned}
\dot{V}_i &\le -k_{xi}\bar{e}_{xi}^2 - k_{yi}\bar{e}_{yi}^2 - k_{\theta i}\sin^2\bar{e}_{\theta i} - k_{vi}\bar{e}_{vi}^2 + \left|\tilde{\Delta}_{xi} + \xi_{xi}\right| |\bar{e}_{xi}| \\
&\quad + \left|\tilde{\Delta}_{yi} + \xi_{yi}\right| |\bar{e}_{yi}| + \left|\tilde{\Delta}_{\theta i}\right| |\sin\bar{e}_{\theta i}| + |\Delta_{vi}|\,|\bar{e}_{vi}| - \bar{k}_{xi}\,|\bar{e}_{xi}| \\
&\quad - \bar{k}_{yi}\,|\bar{e}_{yi}| - \bar{k}_{\theta i}\,|\sin\bar{e}_{\theta i}| - \bar{k}_{vi}\,|\bar{e}_{vi}| + 4\exp(-\varsigma t).
\end{aligned} \tag{33}$$

As $\bar{k}_{xi} > \left|\tilde{\Delta}_{xi} + \xi_{xi}\right|$, $\bar{k}_{yi} > \left|\tilde{\Delta}_{yi} + \xi_{yi}\right|$, $\bar{k}_{\theta i} > \left|\tilde{\Delta}_{\theta i}\right|$, and $\bar{k}_{vi} > |\Delta_{vi}|$ are satisfied, (33) can be written as

$$\dot{V}_i \le -k_{xi}\bar{e}_{xi}^2 - k_{yi}\bar{e}_{yi}^2 - k_{\theta i}\sin^2\bar{e}_{\theta i} - k_{vi}\bar{e}_{vi}^2 + 4\exp(-\varsigma t). \tag{34}$$

When the total Lyapunov candidate function for all the vehicles in the platoon system is selected as $V = \sum_{i=1}^{n} V_i$, its time derivative can be expressed using (34) as

$$\dot{V} \le \sum_{i=1}^{n}\left[-k_{xi}\bar{e}_{xi}^2 - k_{yi}\bar{e}_{yi}^2 - k_{\theta i}\sin^2\bar{e}_{\theta i} - k_{vi}\bar{e}_{vi}^2 + 4\exp(-\varsigma t)\right]. \tag{35}$$

Integrating (35) yields

$$\begin{aligned}
0 \le V(t) < V(0) - \sum_{i=1}^{n}\int_0^t \Big[k_{xi}\bar{e}_{xi}^2(\tau) + k_{yi}\bar{e}_{yi}^2(\tau) + k_{vi}\bar{e}_{vi}^2(\tau) \\
+ k_{\theta i}\sin^2\bar{e}_{\theta i}(\tau)\Big]\,d\tau + 4n/\varsigma
\end{aligned} \tag{36}$$

where $4n/\varsigma$ is a finite positive constant. Hence, it follows from (36) that $\bar{e}_{xi}, \bar{e}_{yi}, \bar{e}_{\theta i}, \bar{e}_{vi} \in L_2 \cap L_\infty$ holds, and $\dot{\bar{e}}_{xi}, \dot{\bar{e}}_{yi}, \dot{\bar{e}}_{\theta i}, \dot{\bar{e}}_{vi} \in L_\infty$ follows from (21), (29), and Assumptions 1–4, which implies that $\bar{e}_{xi}$, $\bar{e}_{yi}$, $\bar{e}_{\theta i}$, and $\bar{e}_{vi}$ asymptotically converge to zero according to Barbalat's lemma [37].

In addition, the coupled relative spacing errors in (8) are rewritten as $\bar{e}_x = Qe_x$ and $\bar{e}_y = Qe_y$, as mentioned in Remark 4, where

$$Q = \begin{bmatrix} \lambda & -q & \cdots & 0 & 0 \\ 0 & \lambda & -q & \cdots & 0 \\ & & \vdots & & \\ 0 & 0 & \cdots & \lambda & -q \\ 0 & 0 & \cdots & 0 & \lambda \end{bmatrix}. \tag{37}$$

Because $\lambda > 0$ is constant, the matrix $Q \in R^{n\times n}$ is invertible. Therefore, $\bar{e}_x = 0$ and $\bar{e}_y = 0$ are equivalent to $e_x = 0$ and $e_y = 0$, respectively, for all vehicles in the platoon. Consequently, the asymptotic convergence of $\bar{e}_x$ and $\bar{e}_y$ implies the asymptotic convergence of e_x and e_y. ■

Remark 8: Based on Lemma 1, which guarantees asymptotic convergence of $\tilde{\Delta}_{xi}$, $\tilde{\Delta}_{yi}$, and $\tilde{\Delta}_{\theta i}$ to zero, and the boundedness of the available variables ξ_{xi} and ξ_{yi} in (26), $\bar{k}_{xi}$, $\bar{k}_{yi}$, and $\bar{k}_{\theta i}$ can be appropriately selected to satisfy $\bar{k}_{xi} > \left|\tilde{\Delta}_{xi} + \xi_{xi}\right|$, $\bar{k}_{yi} > \left|\tilde{\Delta}_{yi} + \xi_{yi}\right|$, and $\bar{k}_{\theta i} > \left|\tilde{\Delta}_{\theta i}\right|$. Additionally, setting $\bar{k}_{vi}$ to a sufficiently large value to satisfy $\bar{k}_{vi} > |\Delta_{vi}|$ is possible because Δ_{vi} in (27) is bounded by Assumptions 1–4.

Remark 9: In many robust control methods [7], [8], [26], chattering is mitigated by replacing a discontinuous signum function with a saturation or sigmoid function, which often results in only ultimate boundedness of the tracking errors rather than asymptotic convergence. In contrast, the proposed robust terms (i.e., the second term on the right-hand side of each row in (22) and (28)), inspired by [36], reduce chattering by smoothly modulating the magnitude of ς, while still guaranteeing asymptotic convergence of the posture and velocity errors to zero, as established in Theorem 1.

Next, we analyze the mesh stability of the proposed platoon system shown in Fig. 1 using Theorem 2.

Theorem 2: (Mesh Stability of Platoon System Using Proposed Robust Platoon Control): If the coupled relative spacing errors with $0 < \lambda \le q$ in (8) converge to zero, then the mesh stability of the platoon system shown in Fig. 1 can be guaranteed.

Proof: According to Theorem 1, (8) converges to zero regardless of the initial condition, thereby leading to $\lambda e_{xi} - qe_{xi+1} = 0$ and $\lambda e_{yi} - qe_{yi+1} = 0$, which can be transformed using the Laplace transform into $\lambda E_{xi}(s) - qE_{xi+1}(s) = 0$ and $\lambda E_{yi}(s) - qE_{yi+1}(s) = 0$, respectively. Consequently, the error propagation transfer functions, $H_{xi}(s) := E_{xi+1}(s)/E_{xi}(s)$ and $H_{yi}(s) := E_{yi+1}(s)/E_{yi}(s)$, for the x and y axes, respectively, can be derived as

$$H_{xi}(s) = H_{yi}(s) = \begin{cases} \lambda/q & \text{for } i = 1, \cdots, n-1 \\ 0 & \text{for } i = n. \end{cases} \tag{38}$$

Because λ and q in (8) satisfy $0 < \lambda \leq q$ for $i = 1, \cdots, n-1$, which in turn guarantees $|H_x(s)| = |H_y(s)| \leq 1$ for all the vehicles in a platoon, the mesh stability of the entire platoon system shown in Fig. 1 can be guaranteed. ■

We have demonstrated the asymptotic stability of the relative posture errors and mesh stability of the platoon system using Theorems 1 and 2. The performance of the proposed method will be verified through simulations and experiments in Section V.

V. SIMULATION AND EXPERIMENTAL RESULTS

We present simulation and experimental results to verify the control performance of the proposed method by comparing it with the following methods:

- *C1 (proposed method with ISMDOB):* Robust platoon control combining ISMDOB [35] with the proposed robust platoon controller in (28), replacing (17) with $\dot{\hat{\gamma}}_{pi} = 0$.
- *C2 (SMC method) [26]:* A robust distance-based predecessor-following method using the relative posture and SMC designed by replacing (22) and (28) as follows:

$$\begin{aligned} [X_i, Y_i]^T &= -a_i \tanh(\bar{e}_i/a_i) - \bar{a}_i \mathrm{sat}(\bar{e}_i/d_i) \\ &\quad - \lambda[\Phi_{xi}, \Phi_{yi}]^T \\ \omega_i &= -\Phi_{\theta i} - b_i \sin \bar{e}_{\theta i} - \bar{b}_i \mathrm{sat}(\bar{e}_{\theta i}/d_i) \end{aligned} \tag{39}$$

  where $\tanh(\bar{e}_i/a_i) = [\tanh(\bar{e}_{xi}/a_i), \tanh(\bar{e}_{yi}/a_i)]^T$, $\mathrm{sat}(\bar{e}_i/d_i) = [\mathrm{sat}(\bar{e}_{xi}/d_{wi}), \mathrm{sat}(\bar{e}_{yi}/d_{wi})]^T$, and $a_i, \bar{a}_i, b_i, \bar{b}_i, d_i > 0$.
- *C3 (extended look-ahead method) [24]:* Combined longitudinal and lateral platoon control using extended look-ahead approach, as in the proposed method.

As no existing method is available to ensure mesh stability of a bidirectional platoon system using relative postures, we modified the SMC method in [26] to handle the proposed coupled relative posture error dynamics in (10)–(12), establishing method C2, such that its control performance could be compared with that of the proposed method. Furthermore, the effectiveness of the proposed method was confirmed by comparing it to the extended look-ahead method in [24] (method C3), which addressed deviation on a curved path.

TABLE 1. Simulation parameters for initial conditions, AISMDOB, and proposed controllers.

Parameter	Value
Initial postures $[x_i(0), y_i(0), \theta_i(0)]$	[7.7, 4, 0]; [6.6, 3.4, 0]; [5.6, 2.9, 0]; [4.7, 2.5, 0]; [3.9, 2.2, 0]; [3.2, 2, 0]; [2.6, 1.9, 0] (m, m, deg); $i=0,\cdots,6$
Initial velocities	$v_i(0)=3\,\mathrm{m/s}$; $\omega_i(0)=0\,\mathrm{deg/s}$; $i=0,\cdots,6$
AISMDOB	$a_i=2.5$; $b_i=0.001$; $\hat{\gamma}_{pi}(0)=0.01$; $\mu_{pi}=8$; $\eta_{pi}=\bar{\eta}_{pi}=10$ in (15)–(20)
Proposed controller	$l=0.5$ in (2); $\lambda=0.99$, $q=1$ for $i\neq n$, $q=0$ for $i=n$ in (8); $k_{xi}=k_{yi}=1.5$; $k_{\theta i}=5$; $k_{vi}=50$; $\bar{k}_{xi}=\bar{k}_{yi}=\bar{k}_{\theta i}=0.5$; $\bar{k}_{vi}=20$; $\varsigma=0.1$ in (22) and (28)

A. SIMULATION RESULTS

The platoon system for the simulations was composed of six vehicles ($n = 6$) and one virtual vehicle ($i = 0$), as shown in Fig. 1. The initial and velocities for $i = 0, \cdots, 6$ are listed in Table 1. The reference path was generated using $\dot{x}_0 = v_0 \cos\theta_0$, $\dot{y}_0 = v_0 \sin\theta_0$, and $\dot{\theta}_0 = \omega_0$, where $v_0 = 3$ m/s and ω_0 was obtained by integrating the following expression:

$$\dot{\omega}_0(t) = \begin{cases} 40\,\mathrm{deg/s^2}, & 3\,\mathrm{s} \leq t < 4\,\mathrm{s} \text{ and } 16\,\mathrm{s} \leq t < 17\,\mathrm{s} \\ -40\,\mathrm{deg/s^2}, & 9\,\mathrm{s} \leq t < 11\,\mathrm{s} \\ 0\,\mathrm{deg/s^2}, & \text{otherwise.} \end{cases} \tag{40}$$

The use of the reference path generated by (40), including the linear and curved trajectories on a 2D plane shown in Fig. 4, allowed to verify the overall platoon control performance. The mesh stability of the proposed platoon system was further confirmed by setting the kinematic and dynamic disturbances and unmodeled dynamic function in (1) such that $\delta_{vi} = \delta_{\omega i} = \delta_{ai} + f_i(x_i, y_i, v_i, t) = 0.5\sin(t)e^{-(t-10+0.1i)^2}$, as in [8], caused fluctuation of the spacing errors along both the x- and y-axis directions around 10 seconds. Additionally, zero-mean Gaussian noise with a maximum of 2% of the corresponding values was included in the velocity information to demonstrate the robustness of the proposed method under measurement noise. The controller and observer parameters were tuned via trial and error and are summarized in Table 1. For a fair comparison, the control parameters of methods C1–C3 were set to perform well in the absence of kinematic and dynamic disturbances.

Fig. 4 shows the trajectories of the platoon vehicles used in the simulations. Figs. 4(a) and 4(b) show that the platoon vehicles suitably followed the reference path in linear motion. However, unlike the previous vehicle-following method obtained by setting $\alpha_{i-1} = 0$ in (2) (Fig. 4(a)), in which the vehicles deviated from the reference path during curved motion, all the vehicles in the platoon accurately followed the reference path without deviation during

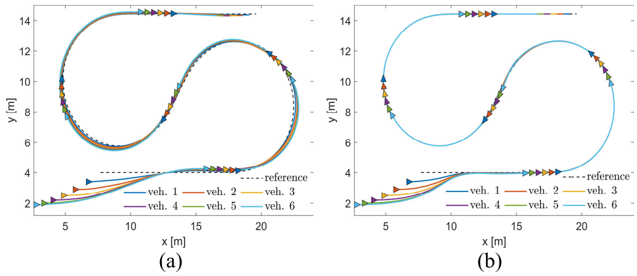

FIGURE 4. Trajectory of platoon vehicles in simulations for (a) previous vehicle-following method with [26] and [34] and (b)proposed method.

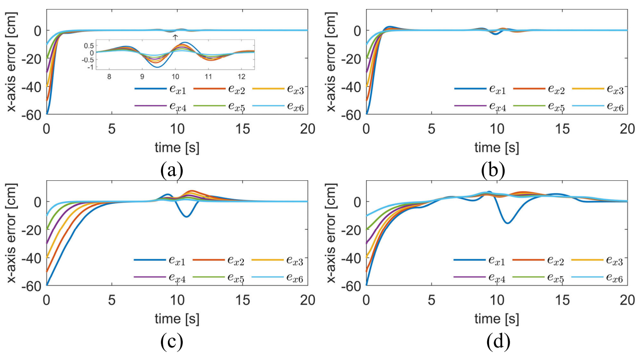

FIGURE 5. Simulation results of x-axis spacing error e_{xi} for (a) proposed method and comparison methods (b) C1, (c) C2 [26], and (d) C3 [24].

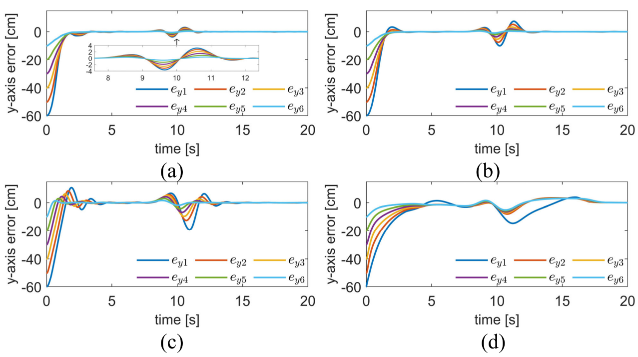

FIGURE 6. Simulation results of y-axis spacing error e_{yi} for (a) proposed method and comparison methods (b) C1, (c) C2 [26], and (d) C3 [24].

curved motion when using the proposed method, as shown in Fig. 4(b).

Figs. 5–7 compare relative posture errors e_{xi}, e_{yi}, and $e_{\theta i}$, respectively, of the proposed method with those of methods C1, C2, and C3 in the simulations. The relative spacing errors of the proposed method shown in Figs. 5(a) and 6(a) asymptotically converged to zero within approximately 1.5 s without overshoot for all the vehicles in the platoon through the compensation for both the spacing errors of the rear vehicle and lumped disturbances. Notably, the relative spacing errors in Figs. 5(a) and 6(a) did not propagate to the rear vehicle along neither the x- nor y-axis direction, as shown in the enlarged views from 8 s to 12 s, confirming the mesh stability of the proposed platoon system. Fig. 7(a) shows the heading

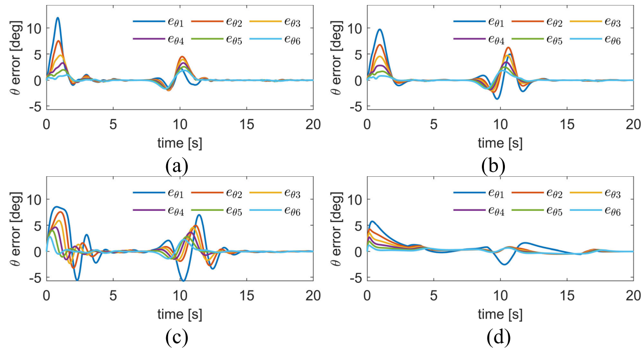

FIGURE 7. Simulation results of heading angle error $e_{\theta i}$ for (a) proposed method and comparison methods (b) C1, (c) C2 [26], and (d) C3 [24].

angle errors of the proposed method, which asymptotically converged to zero. The relative spacing errors of method C1 in Figs. 5(b) and 6(b) exhibited an overshoot of approximately 3 cm during the transient response and fluctuations owing to inadequate compensation for the disturbances at approximately 10 s. The heading angle errors of method C1 shown in Fig. 7(b) converged asymptotically to zero. Both the relative spacing errors of methods C2, shown in Figs. 5(c) and 6(c), and C3, shown in Figs. 5(d) and 6(d), indicate a poor transient response owing to the lack of compensation for both the spacing errors of the rear vehicle and disturbances, leading to considerable fluctuations around 10 s. The heading angle errors of method C2 shown in Fig. 7(c) asymptotically converged to zero with some fluctuations, and those of method C3 in Fig. 7(d) exhibited an overshoot of approximately 5°.

Table 2 lists the average values of the mean absolute error (MAE) and root mean square error (RMSE) for the relative posture errors obtained from the simulations using the proposed method and comparison methods C1, C2, and C3, where the average values of the MAE and RMSE are given by

$$
\begin{aligned}
e_{xy}^{\mathrm{MAE}} &= \sum_{i=1}^{n}\sum_{k=1}^{N}\frac{|e_{xi}(k)|+|e_{xi}(k)|}{nN},\\
e_{\theta}^{\mathrm{MAE}} &= \sum_{i=1}^{n}\sum_{k=1}^{N}\frac{|e_{\theta i}(k)|}{nN}\\
e_{xy}^{\mathrm{RMSE}} &= \sum_{i=1}^{n}\sqrt{\sum_{k=1}^{N}\frac{e_{xi}^2(k)+e_{yi}^2(k)}{n^2N}},\\
e_{\theta}^{\mathrm{RMSE}} &= \sum_{i=1}^{n}\sqrt{\sum_{k=1}^{N}\frac{e_{\theta i}^2(k)}{n^2N}}.
\end{aligned}
\tag{41}
$$

Table 2 shows that the average MAE and RMSE values of the proposed method are smaller than those of methods C1, C2, and C3 in most cases.

Fig. 8 shows longitudinal velocity error $\bar{e}_{vi}$ and control input u_i obtained during the simulation. Because methods C2 and C3 use velocity commands as control inputs without considering velocity errors, and the results of method C1 are

TABLE 2. Simulation results of average MAE and RMSE for relative posture errors obtained from evaluated methods.

Method	MAE		RMSE	
	e_{xy}^{MAE} [cm]	$e_{\theta}^{\mathrm{MAE}}$ [deg]	e_{xy}^{RMSE} [cm]	$e_{\theta}^{\mathrm{RMSE}}$ [deg]
Proposed	2.7423	0.4849	7.6831	1.1672
C1	3.1238	0.5778	7.9090	1.2596
C2 [26]	5.1770	0.7757	9.0313	1.5146
C3 [24]	8.6062	0.5288	10.0842	0.7949

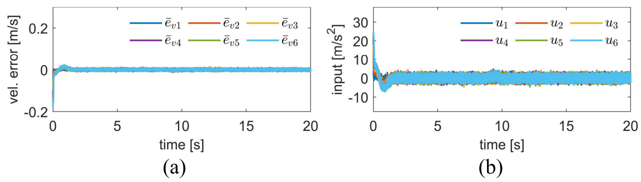

FIGURE 8. Simulation results of (a) longitudinal velocity error $\bar{e}_{vi}$ and (b) control input u_i of proposed method.

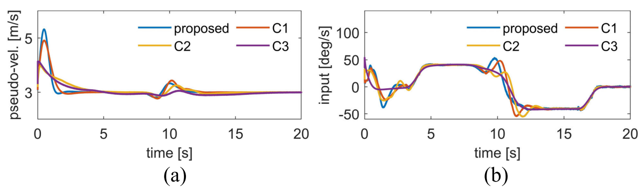

FIGURE 9. Simulation results of (a) pseudo longitudinal velocity v_{pse3} and (b) angular velocity control input ω_3.

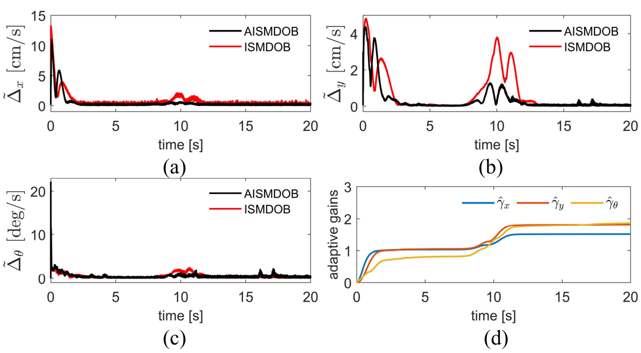

FIGURE 10. Simulation results of estimation errors and adaptive gains. (a) x-axis estimation error $\tilde{\Delta}_x$ and (b) y-axis estimation error $\tilde{\Delta}_y$. (c) θ-axis estimation error $\tilde{\Delta}_\theta$. (d) Adaptive gains $\hat{\gamma}_x$, $\hat{\gamma}_y$, and $\hat{\gamma}_\theta$.

similar to those of the proposed method, only the results of the proposed method are shown in Fig. 8. The longitudinal velocity errors shown in Fig. 8(a) asymptotically converged to zero. The control inputs in Fig. 8(b) reflected the Gaussian random noise applied to the velocity information, which did not affect the control performance. Figs. 9(a) and 9(b) depict the pseudo longitudinal velocity and angular velocity input of the third vehicle in the six-vehicle platoon, respectively, as a representative example for comparison of the methods. From Figs. 8(b) and 9(b), it can be observed that the control inputs generated by the proposed method had appropriate magnitudes.

Fig. 10 shows the estimation errors of the kinematic disturbances obtained from the AISMDOB and ISMDOB as well as

TABLE 3. Simulation results of MAE, RMSE, peak error, and settling time for estimation errors of AISMDO Band ISMDOB [35].

Observer	$\tilde{\Delta}_x$	$\tilde{\Delta}_y$	$\tilde{\Delta}_\theta$	$\tilde{\Delta}_x$	$\tilde{\Delta}_y$	$\tilde{\Delta}_\theta$
	MAE [cm/s, deg/s] RMSE [cm/s, deg/s]			Settling time [s] Peak [cm/s, deg/s]		
AISMDOB	0.474	0.365	0.489	1.09	2.67	1.43
	1.251	0.839	0.820	11.003	4.374	22.061
ISMDOB	0.750	0.655	0.518	1.68	3.49	1.47
	1.515	1.257	0.865	13.155	4.819	14.922

the adaptive gains in the simulations. Figs. 10(a)–10(c) show $\tilde{\Delta}_x$, $\tilde{\Delta}_y$, and $\tilde{\Delta}_\theta$, respectively, where $\tilde{\Delta}_p = \sum_{i=1}^{n} \left|\tilde{\Delta}_{pi}\right| / n$ for $p = x, y, \theta$. The estimation errors of the AISMDOB were smaller than those of the ISMDOB, particularly under kinematic disturbances. It should be noted that except for the constant γ_{pi} set to 0.01, the remaining observer gains of the ISMDOB are identical to those of the AISMDOB. Fig. 10(d) shows the adaptive gains represented as $\hat{\gamma}_p = \sum_{i=1}^{n} \hat{\gamma}_{pi} / n$, with the adaptive gains increasing until approximately 10 s and finally converging to 1.51, 1.81, and 1.86, respectively.

Table 3 lists the MAE and RMSE for the estimation errors of the AISMDOB and ISMDOB in the simulations. The MAE and RMSE of the estimation errors are given by

$$\mathrm{MAE} = \frac{1}{N} \sum_{k=k_0}^{k_0+N-1} \left|\tilde{\Delta}_p(k)\right|, \quad \mathrm{RMSE} = \sqrt{\frac{1}{N} \sum_{k=k_0}^{k_0+N-1} \tilde{\Delta}_p^2(k)} \tag{42}$$

where k_0 corresponds to $t = 5$ s. To compare the transient responses, Table 3 also reports the peak error and settling time over $t \in [0, 5]$ s. The settling time is defined as the time for $\left|\tilde{\Delta}_p\right|$ to return to and remain within the steady-state noise band $\varepsilon_p := 3\sigma_p$ where σ_p denotes the standard deviation computed over a steady interval. As shown in Table 3, AISMDOB yields lower MAE and RMSE than ISMDOB, and its transient metrics indicate improved behavior, particularly in the translational components $\tilde{\Delta}_x$ and $\tilde{\Delta}_y$.

We further validate the effectiveness of the proposed method and its platoon control performance through the experimental results.

B. EXPERIMENTAL SETUP AND RESULTS

To validate the real-time performance of the proposed method, the proposed controller was implemented and experimentally evaluated in real time using three vehicles equipped with OpenCR microcontroller units (MCUs) and XM430-W210 servomotors, as shown in Fig. 11. The proposed control algorithm was executed in real time on a laptop running MATLAB/Simulink integrated with the Robot Operating System (ROS), and the computed vehicle commands were transmitted to the vehicles via ROS-based serial communication. The vehicles in the platoon were differential-drive mobile robots, as those used in [24], [26], and they were

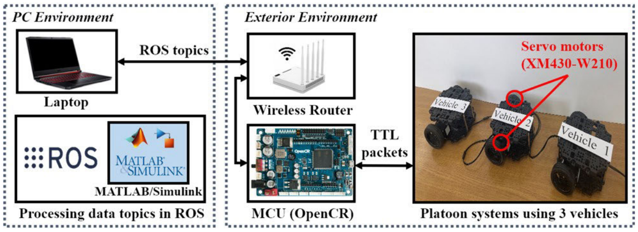

FIGURE 11. **Experimental setup of bidirectional platoon system.**

controlled by providing velocity inputs to the right and left wheels, denoted as ω_{ri} and ω_{li}, respectively. The transformation of pseudo longitudinal velocity v_{psei} and angular velocity input ω_i into the wheel velocity inputs can be determined as follows:

$$\omega_{ri} = \frac{1}{r_i}\left(v_{psei} + \frac{R_i\omega_i}{2}\right), \quad \omega_{li} = \frac{1}{r_i}\left(v_{psei} - \frac{R_i\omega_i}{2}\right) \quad (43)$$

where the wheel radius and distance between the wheels were $r_i = 0.03$m and $R_i = 0.16$m, respectively.

The initial positions were set as $[x_0(0), \cdots, x_3(0)] = [81, 51, 24, 0]$ cm and $[y_0(0), \cdots, y_3(0)] = [21, 11, 4, 0]$ cm, while the initial heading angle was set as $\theta_i(0) = 0$ deg, and the initial velocities were set as $v_i(0) = 15$ cm/s and $\omega_i(0) = 0$ deg$/$s for $i = 0, \cdots, 3$. To support the simulation results described in Section V-A, a reference path similar to that described by (40) was adopted in the experiments, involving both linear and curved motions, with $v_0 = 15$cm/s and ω_0 obtained by integrating the following expression:

$$\dot{\omega}_0(t) = \begin{cases} 10.31 \text{ deg}/\text{s}^2, & 15\text{ s} \le t < 16\text{ s and } 64\text{ s} \le t < 65\text{ s} \\ -10.31 \text{ deg/s}^2, & 39\text{ s} \le t < 41\text{ s} \\ 0 \text{ deg/s}^2, & \text{otherwise.} \end{cases} \quad (44)$$

To demonstrate the mesh stability of the platoon system, disturbances were included as $\delta_{vi} = \delta_{\omega i} = 0.05\sin(t)\, e^{-(0.3t-12+0.3i)^2}$ in (1). The experimental parameters were fine-tuned via trial and error and set as follows: $l = 0.2$ in (2), $\hat{\gamma}_{pi}(0) = 0.0001$, $\mu_{pi} = 10$, and $\eta_{pi} = \bar{\eta}_{pi} = 3$ in (15)–(20), $k_{xi} = k_{yi} = 0.5$, $k_{\theta i} = 1.5$, $\bar{k}_{\theta i} = 1$, and $\varsigma = 0.001$ in (22) and (28), $a_i = b_i = 0.5$ and $\bar{a}_i = \bar{b}_i = 0.01$ in (39), and the remaining parameters were the same as those reported in Section V-A.

Fig. 12 shows the trajectories of the platoon vehicles in the experiments. Consistent with the simulation results in Fig. 4, all vehicles using the proposed method, as illustrated in Fig. 12(b), accurately adhered to the reference path in both linear and curved motions. In contrast, vehicles utilizing the previous vehicle-following method, depicted in Fig. 12(a), deviated from the reference path during curved motion.

Figs. 13–15 show relative posture errors e_{xi}, e_{yi}, and $e_{\theta i}$, respectively, for the proposed method and comparison methods C1, C2, and C3. The spacing errors of the

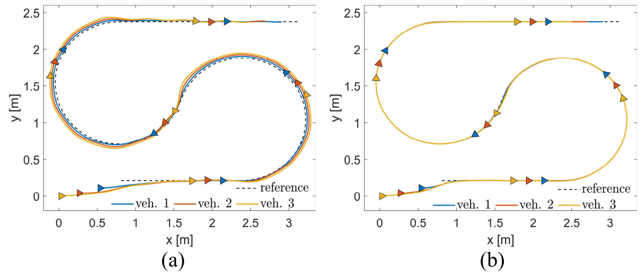

FIGURE 12. **Trajectory of platoon vehicles in experiments for (a) previous vehicle-following method with $\alpha_{i-1} = 0$ [26], [34] and (b) proposed method.**

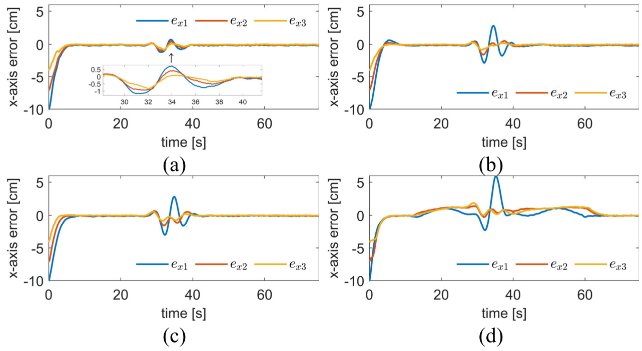

FIGURE 13. **Experimental results of x-axis spacing error e_{xi} for (a) proposed method and comparison methods (b) C1, (c) C2 [26], and (d) C3 [24].**

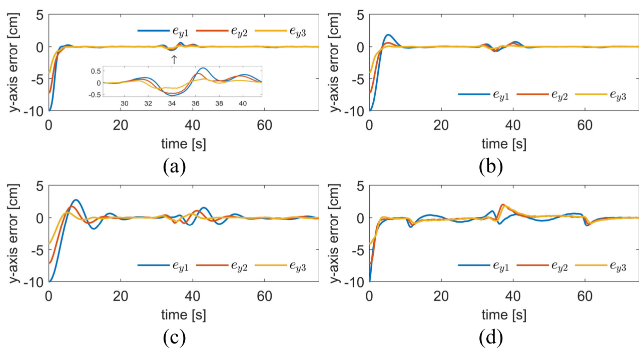

FIGURE 14. **Experimental results of y-axis spacing error e_{yi} for (a) proposed method and comparison methods (b) C1, (c) C2 [26], and (d) C3 [24].**

proposed method shown in Figs. 13(a) and 14(a) asymptotically converged to zero without overshooting owing to effective compensation for kinematic disturbances. Moreover, as shown in the enlarged views of Figs. 13(a) and 14(a), the spacing errors did not propagate to the rear vehicle along neither the x- nor y-axis direction, being consistent with the simulation results shown in Figs. 5(a) and 6(a) and indicating the guaranteed mesh stability of the proposed control method. The heading angle errors of the proposed method shown in Fig. 15(a) asymptotically converged to zero. The relative spacing errors of method C1 shown in Figs. 13(b) and 14(b) initially exhibited a slight overshoot of 1.8 cm

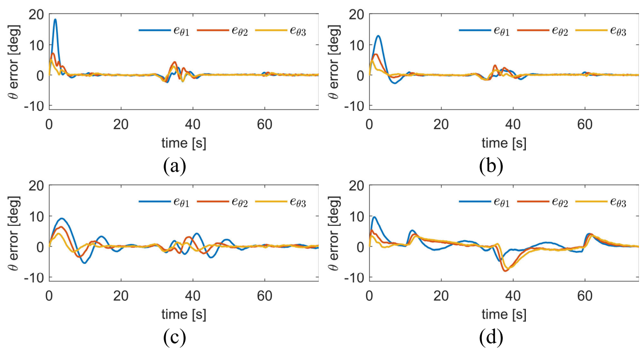

FIGURE 15. Experimental results of heading angle error $e_{\theta i}$ for (a) proposed method and comparison methods (b) C1, (c) C2 [26], and (d) C3 [24].

TABLE 4. Experimental results of average MAE and RMSE for relative posture errors obtained from evaluated methods.

Method	MAE		RMSE	
	e_{xy}^{MAE} [cm]	$e_{\theta}^{\mathrm{MAE}}$ [deg]	e_{xy}^{RMSE} [cm]	$e_{\theta}^{\mathrm{RMSE}}$ [deg]
Proposed	0.5232	0.4973	1.2830	1.4385
C1	0.6387	0.5486	1.3863	1.4026
C2 [26]	0.8528	0.9556	1.5319	1.6652
C3 [24]	1.2335	1.4187	1.6027	2.1611

and asymptotically converged to zero, with some fluctuations occurring around 34 s owing to the insufficient compensation of disturbances. The heading angle errors of method C1 shown in Fig. 15(b) asymptotically converged to zero. In the relative spacing errors of method C2 shown in Figs. 13(c) and 14(c), the x-axis error converged to zero, whereas the y-axis error had an overshoot of 2.7 cm, both exhibiting fluctuations affected by disturbances. The relative spacing errors of method C3 shown in Figs. 13(d) and 14(d) initially converged smoothly to zero, but then exhibited significant fluctuations. The heading angle errors of methods C2 and C3 shown in Figs. 15(c) and 15(d) had small initial overshoots, but they continued to fluctuate owing to disturbances.

Table 4 lists the average MAE and RMSE values in (41) for the relative posture errors of the proposed method and comparison methods C1, C2, and C3. Notably, both the average values of the proposed method were smaller than those of methods C1, C2, and C3 across most metrics, indicating the superior platoon control performance of the proposed method compared with the other methods.

Fig. 16 shows the pseudo longitudinal velocity and angular velocity input of the second vehicle in the platoon for the proposed method and comparison methods C1, C2, and C3, which correspond to the control inputs described by (43). Because $\bar{e}_{vi}$ could be designed to converge to zero through a simple proportional–integral–derivative (PID) controller embedded in the servomotors mounted on the platoon vehicles, as illustrated in Fig. 11, (43) could be applied directly to the vehicles, and the control performance of the proposed method and method C1 could be fairly compared with that of

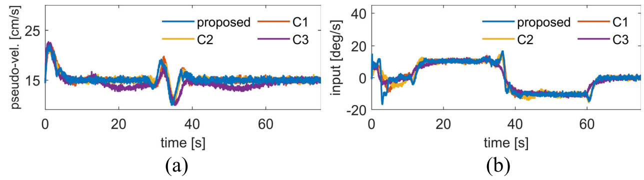

FIGURE 16. Experimental results of (a) pseudo longitudinal velocity input v_{pse2} and (b) angular velocity control input ω_2.

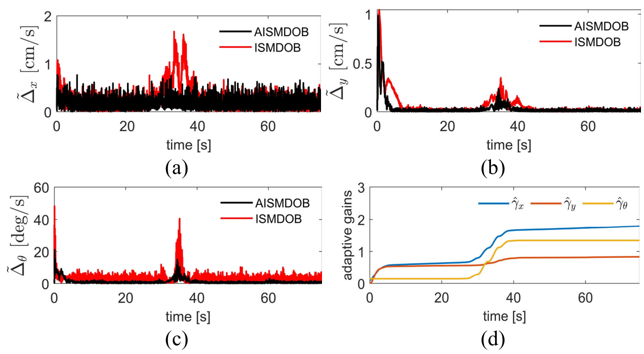

FIGURE 17. Experimental results of estimation errors and adaptive gains. (a) x-axis estimation error $\tilde{\Delta}_x$ and (b) y-axis estimation error $\tilde{\Delta}_y$. (c) θ-axis estimation error $\tilde{\Delta}_\theta$. (d) Adaptive gains $\hat{\gamma}_x$, $\hat{\gamma}_y$, and $\hat{\gamma}_\theta$.

TABLE 5. Experimental results of MAE, RMSE, peak error, and settling time for estimation errors of AISMDOB and ISMDOB [35].

Observer	$\tilde{\Delta}_x$	$\tilde{\Delta}_y$	$\tilde{\Delta}_\theta$	$\tilde{\Delta}_x$	$\tilde{\Delta}_y$	$\tilde{\Delta}_\theta$
	MAE [cm/s, deg/s] RMSE [cm/s, deg/s]			Settling time [s] Peak [cm/s, deg/s]		
AISMDOB	0.184 0.216	0.032 0.091	1.147 2.012	0.64 0.776	3.95 0.986	3.38 21.090
ISMDOB	0.244 0.344	0.059 0.133	3.107 4.196	1.74 1.079	7.13 1.044	1.60 49.074

methods C2 and C3 that used velocity commands as control inputs. It was confirmed from Fig. 16 that the control inputs in the experiment were generated with appropriate magnitudes.

Fig. 17 shows the estimation errors of the AISMDOB and ISMDOB as well as the adaptive gains in the experiments. As shown in Figs. 17(a)–17(c), all metrics of the AISMDOB were smaller than those of the conventional ISMDOB, implying that the AISMDOB achieved superior estimation performance. Fig. 17(d) shows the adaptive gains in the experiments. The adaptive gains increased at the beginning and around 34 s and finally converged to 1.78, 0.84, and 1.34.

Table 5 lists the MAE and RMSE values computed using (42) for the estimation errors in the experiments, where k_0 corresponds to $t = 10$ s. Table 5 also provides the peak error and settling time over $t \in [0, 10]$ s, using the same definitions as in the simulation results. The AISMDOB yields lower errors than ISMDOB and shows improved transient behavior.

The simulation and experimental results presented in this section validate the effectiveness of the proposed method through comparison with three existing methods (proposed method with ISMDOB [35], SMC method [26], and extended look-ahead method [24]). The proposed controller exhibits comparable performance to the comparison methods when external disturbances are absent or negligible; however, under disturbance conditions, it yields smaller overshoot, faster recovery, and reduced steady-state errors, indicating enhanced disturbance-rejection capability. In addition, the proposed method maintains more accurate trajectory tracking during cornering maneuvers than previous vehicle-following methods [26], [34]. These observations suggest that the main advantage of the proposed AISMDOB-based design lies in its robust disturbance rejection and curved-path tracking performance.

VI. CONCLUSION

In this paper, a coupled relative posture error-based robust bidirectional platoon control method using an AISMDOB is proposed to ensure mesh stability of a bidirectional platoon system subject to kinematic and dynamic disturbances. Coupled relative posture error variables are introduced to derive the coupled relative posture error dynamics on a 2D plane using only relative posture information, which enables cost-effective and practical implementation without relying on global positioning. Based on these dynamics, a novel AISMDOB-based bidirectional platoon controller is designed to guarantee the asymptotic convergence of both relative spacing and heading angle errors while compensating for kinematic and dynamic disturbances. The mesh stability of the platoon system is ensured by extending one-dimensional platoon control concepts to simultaneously handle error propagation in both the longitudinal and lateral directions. Simulation and experimental results validate the effectiveness of the proposed method and demonstrate effective tracking and disturbance-rejection performance compared with existing methods, including the conventional ISMDOB-based method, an SMC method, and an extended look-ahead method.

The proposed method presents several limitations. First, the proposed method assumes that accurate curvature information of the preceding vehicle path is available to define the target posture. In practice, this information is obtained from onboard sensing or road-geometry data and manifests in the error dynamics as a bounded disturbance; consequently, the AISMDOB can compensate for moderate curvature errors, but significant estimation inaccuracies may still degrade tracking performance. Second, model mismatches such as moderate load variations and unmodeled tire dynamics are also treated as lumped disturbances and can be handled within the present AISMDOB framework, whereas significant or rapidly varying parameter changes may require re-tuning of the AISMDOB gains. Furthermore, a bidirectional communication topology without packet loss is assumed in this study, and the influence of more general topologies and communication uncertainties has not been fully addressed.

Future work includes extending the proposed framework to handle communication uncertainties and more general network topologies such as ring configurations, and analyzing the impact of curvature estimation errors. We also plan to enhance the AISMDOB to robustly accommodate large model mismatches and to introduce systematic gain tuning methods (e.g., Bayesian optimization), and validate the method on larger-scale heterogeneous platoons in more complex road networks.

REFERENCES

[1] F. Viadero-Monasterio, M. Meléndez-Useros, M. Jiménez-Salas, and B. L. Boada, "Robust adaptive heterogeneous vehicle platoon control based on disturbances estimation and compensation," *IEEE Access*, vol. 12, pp. 96924–96935, 2024.

[2] M. Mu, J. Zhang, C. Wang, J. Zhang, and C. Yang, "String stability and platoon safety analysis of a new car-following model considering a stabilization strategy," *IEEE Access*, vol. 9, pp. 111336–111345, 2021.

[3] K. B. Devika, G. Rohith, and S. C. Subramanian, "Potential function-based string stable controller for heavy road vehicle platoons," *IEEE Access*, vol. 9, pp. 156274–156282, 2021.

[4] K. B. Devika, G. Rohith, V. R. Shreya Yellapantula, and S. C. Subramanian, "A dynamics-based adaptive string stable controller for connected heavy road vehicle platoon safety," *IEEE Access*, vol. 8, pp. 209886–209903, 2020.

[5] S. Baldi, D. Liu, V. Jain, and W. Yu, "Establishing platoons of bidirectional cooperative vehicles with engine limits and uncertain dynamics," *IEEE Trans. Intell. Transp. Syst.*, vol. 22, no. 5, pp. 2679–2691, May 2021.

[6] H. Xing, J. Ploeg, and H. Nijmeijer, "Compensation of communication delays in a cooperative ACC system," *IEEE Trans. Veh. Technol.*, vol. 69, no. 2, pp. 1177–1189, Feb. 2020.

[7] J.-W. Kwon and D. Chwa, "Adaptive bidirectional platoon control using a coupled sliding mode control method," *IEEE Trans. Intell. Transp. Syst.*, vol. 15, no. 5, pp. 2040–2048, Oct. 2014.

[8] J. Boo and D. Chwa, "Integral sliding mode control-based robust bidirectional platoon control of vehicles with the unknown acceleration and mismatched disturbance," *IEEE Trans. Intell. Transp. Syst.*, vol. 24, no. 10, pp. 10881–10894, Oct. 2023.

[9] Z. Gao, Z. Sun, and G. Guo, "Adaptive predefined-time tracking control for vehicular platoons with finite-time global prescribed performance independent of initial conditions," *IEEE Trans. Veh. Technol.*, vol. 73, no. 11, pp. 16254–16267, Nov. 2024.

[10] A. Khalil, K. F. Aljanaideh, and M. A. Janaideh, "On connected autonomous vehicles with unknown human driven vehicles effects using transmissibility operators," *IEEE Trans. Autom. Sci. Eng.*, vol. 20, no. 3, pp. 1876–1889, Jul. 2023.

[11] P. Zhu, S. Jin, X. Bu, and Z. Hou, "Distributed data-driven control for a connected autonomous vehicle platoon subjected to false data injection attacks," *IEEE Trans. Autom. Sci. Eng.*, vol. 21, no. 4, pp. 7527–7538, Oct. 2024.

[12] S. Solyom, A. Idelchi, and B. B. Salamah, "Lateral control of vehicle platoons," in *Proc. IEEE Int. Conf. Syst., Man, Cybern.*, Oct. 2013, pp. 4561–4565.

[13] O. Hassanain, M. Alirezaei, J. Ploeg, and N. V. de Wouw, "String-stable automated steering in cooperative driving applications," *Vehicle Syst. Dyn.*, vol. 58, no. 5, pp. 826–842, Apr. 2020.

[14] S. Shohani, A. Yazdizadeh, and A. Sadeghzadeh, "Lateral string stabilization of connected vehicles with time-varying longitude velocity based on gain-scheduling approach," *Eur. J. Control*, vol. 75, Jan. 2024, Art. no. 100925.

[15] I. Papadimitriou and M. Tomizuka, "Lateral control of platoons of vehicles on highways: The autonomous following based approach," *Int. J. Vehicle Design*, vol. 36, no. 1, pp. 24–37, Sep. 2004.

[16] N. Zhang, S. Nazari, J. Chen, X. Xu, and H. Zhang, "Bayesian optimization for automatic tuning of an energy aware 2-D vehicle platoon," *IEEE Trans. Intell. Vehicles*, vol. 9, no. 11, pp. 7380–7391, Nov. 2024.

[17] B. Li, Y. Zhang, Y. Feng, Y. Zhang, Y. Ge, and Z. Shao, "Balancing computation speed and quality: A decentralized motion planning method for cooperative lane changes of connected and automated vehicles," *IEEE Trans. Intell. Vehicles*, vol. 3, no. 3, pp. 340–350, Sep. 2018.

[18] Z. Zhou, F. Zhu, D. Xu, B. Chen, S. Guo, and Y. Dai, "Event-triggered multi-lane fusion control for 2-D vehicle platoon systems with distance constraints," *IEEE Trans. Intell. Vehicles*, vol. 8, no. 2, pp. 1498–1511, Feb. 2023.
[19] H. Zhao, D. Sun, M. Zhao, Q. Pu, and C. Tang, "Combined longitudinal and lateral control for heterogeneous nodes in mixed vehicle platoon under V2I communication," *IEEE Trans. Intell. Transp. Syst.*, vol. 23, no. 7, pp. 6751–6765, Jul. 2022.
[20] L. Xu, W. Zhuang, G. Yin, C. Bian, and H. Wu, "Modeling and robust control of heterogeneous vehicle platoons on curved roads subject to disturbances and delays," *IEEE Trans. Veh. Technol.*, vol. 68, no. 12, pp. 11551–11564, Dec. 2019.
[21] A. Bayuwindra, J. Ploeg, E. Lefeber, and H. Nijmeijer, "Combined longitudinal and lateral control of car-like vehicle platooning with extended look-ahead," *IEEE Trans. Control Syst. Technol.*, vol. 28, no. 3, pp. 790–803, May 2020.
[22] H. Min, X. Wu, C. Cheng, and X. Zhao, "Kinematic and dynamic vehicle model-assisted global positioning method for autonomous vehicles with low-cost GPS/camera/in-vehicle sensors," *Sensors*, vol. 19, no. 24, p. 5430, Dec. 2019.
[23] S. Wei, Y. Zou, X. Zhang, T. Zhang, and X. Li, "An integrated longitudinal and lateral vehicle following control system with radar and vehicle-to-vehicle communication," *IEEE Trans. Veh. Technol.*, vol. 68, no. 2, pp. 1116–1127, Feb. 2019.
[24] A. Bayuwindra, E. Lefeber, J. Ploeg, and H. Nijmeijer, "Extended look-ahead tracking controller with orientation-error observer for vehicle platooning," *IEEE Trans. Intell. Transp. Syst.*, vol. 21, no. 11, pp. 4808–4821, Nov. 2020.
[25] A. Bayuwindra, L. Wonohito, and B. R. Trilaksono, "Design of DDPG-based extended look-ahead for longitudinal and lateral control of vehicle platoon," *IEEE Access*, vol. 11, pp. 96648–96660, 2023.
[26] D. Chwa, "Robust distance-based tracking control of wheeled mobile robots using vision sensors in the presence of kinematic disturbances," *IEEE Trans. Ind. Electron.*, vol. 63, no. 10, pp. 6172–6183, Oct. 2016.
[27] S. Khodadadi, T. K. Tasooji, and H. J. Marquez, "Observer-based secure control for vehicular platooning under DoS attacks," *IEEE Access*, vol. 11, pp. 20542–20552, 2023.
[28] K. R. Surur, A. Alshakhs, and M. Faizan Mysorewala, "Merging maneuver technique for an adaptive autonomous platoon in multi-lane highways," *IEEE Access*, vol. 12, pp. 157761–157774, 2024.
[29] A. Pant, P. Seiler, and K. Hedrick, "Mesh stability of look-ahead interconnected systems," *IEEE Trans. Autom. Control*, vol. 47, no. 2, pp. 403–407, Feb. 2002.
[30] Z. L. Cao, T. Li, and J. Y. Zhang, "Mesh exponential stability of look-ahead interconnected system," *Appl. Mech. Mater.*, vols. 29–32, pp. 847–850, Aug. 2010.
[31] M. Mirabilio, A. Iovine, E. De Santis, M. D. D. Benedetto, and G. Pola, "Scalable mesh stability of nonlinear interconnected systems," *IEEE Control Syst. Lett.*, vol. 6, pp. 968–973, 2022.
[32] M. Qiu, D. Liu, H. Wang, W. Yu, and S. Baldi, "A cooperative implementation of mesh stability in vehicular platoons," *IEEE Trans. Netw. Sci. Eng.*, vol. 10, no. 3, pp. 1537–1550, May 2023.
[33] J. Boo and D. Chwa, "Robust bidirectional platoon control for mesh stability of vehicular systems with uncertain kinematics and dynamics," *IEEE Trans. Intell. Vehicles*, vol. 10, no. 4, pp. 2304–2318, Apr. 2025.
[34] J. Boo and D. Chwa, "Fuzzy integral sliding mode observer-based formation control of mobile robots with kinematic disturbance and unknown leader and follower velocities," *IEEE Access*, vol. 10, pp. 76926–76938, 2022.
[35] D. Chwa, "Integral-sliding-mode-observer-based structure and motion estimation of a single object in general motion using a monocular dynamic camera," *IEEE Access*, vol. 8, pp. 14207–14222, 2020.
[36] W. Meng, Q. Yang, J. Sarangapani, and Y. Sun, "Distributed control of nonlinear multiagent systems with asymptotic consensus," *IEEE Trans. Syst., Man, Cybern., Syst.*, vol. 47, no. 5, pp. 749–757, May 2017.
[37] H. K. Khalil, *Nonlinear Systems*, 3rd ed., Upper Saddle River, NJ, USA: Prentice-Hall, 1996.

JUNSEOK BOO received the B.S., M.S., and Ph.D. degrees in electrical and computer engineering from Ajou University, Suwon, South Korea, in 2018, 2020, and 2025, respectively.

Since 2025, he has been with the Electronics and Telecommunications Research Institute, Daejeon, South Korea, where he is currently a Researcher. His research interests include nonlinear, robust, and adaptive control theories and their applications to robotics; formation control; and underactuated systems, including mobile robots and mobile manipulators.

KANGMIN JO received the B.S. and M.S. degrees in electrical and computer engineering from Ajou University, Suwon, South Korea, in 2021 and 2023, respectively, where he is currently pursuing the Ph.D. degree in electrical and computer engineering.

His research interests include nonlinear, robust, and adaptive control theories and their applications to robotics, underactuated systems, and vision-based systems.

DONGKYOUNG CHWA received the B.S. and M.S. degrees in control and instrumentation engineering and the Ph.D. degree in electrical and computer engineering from Seoul National University, Seoul, South Korea, in 1995, 1997, and 2001, respectively.

From 2001 to 2003, he was a Postdoctoral Researcher with Seoul National University, where he was also a BK21 Assistant Professor, in 2004. Since 2005, he has been with the Department of Electrical and Computer Engineering, Ajou University, Suwon, South Korea, where he is currently a Professor. His research interests include nonlinear, robust, and adaptive control theories and their applications to robotics; underactuated systems, including wheeled mobile robots; underactuated ships; cranes; and guidance and control of flight systems.